UNIVERSITY OF TURKU

Exploring a possible novel way of enterovirus cell-to-cell transmission through tunnelling nanotubes

Master's Thesis
University of Turku
Department of Life Technologies
Molecular Systems Biology
December 2024

Sayma Farabi

Sayma Farabi

The originality of this thesis has been checked in accordance with the University of Turku quality assurance system using Turnitin Originality Check Service. Artificial intelligence tools were used to enhance language quality.

Master's thesis

Subject: Molecular Systems Biology
Author: Sayma Farabi
Title: Exploring a possible novel way of enterovirus cell-to-cell transmission through tunnelling nanotubes
Supervisor(s): PhD. Sisko Tauriainen (Docent), PhD. Petri Susi (Docent)
Number of pages: 54 pages
Date: 05.12.2024

Tunneling nanotubes (TNTs) are intercellular structures that facilitate direct communication between cells. Recent findings revealed that certain viruses can exploit these actin-based structures to facilitate direct cell-to-cell transmission, thereby evading immune system recognition. In this study, the role of TNTs in mediating cell-to-cell transmission of enteroviruses was investigated, providing insights into a novel mechanism of viral spread.

This research aimed to investigate the potential role of TNTs in mediating the intercellular spread of Coxsackievirus A9 and Coxsackievirus B3. Reagents and methodologies were systematically optimized to investigate this novel mechanism. Enteroviruses would represent the first known non-enveloped human virus to exploit this mode of spreading. After virus infection in GMK cells, immunofluorescences and fluorescent small molecules were used to show infection, cellular morphology, formations of TNTs in infected and non-infected cells. To confirm intercellular connectivity via TNTs, split GFP technology was utilized in a way that when different cell populations, harbouring only fragments of GFP or sfCherry, connected to each other, a fluorescent signal could be observed.

A significant increase in TNT formation following viral infection was demonstrated by the findings. Actin staining using Phalloidin confirmed the presence of actin filaments within these cellular protrusions, supporting their identification as TNTs. While some evidence indicated the presence of viral particles within these actin-containing structures, it was not conclusively determined whether the TNTs were open-ended and capable of facilitating viral transmission to neighbouring cells.

Keywords: enterovirus, fluorescent microscopy, green monkey kidney cells (GMK), split GFP, tunneling nanotubes

Contents

Abbreviations

BSA	Bovine serum albumin
CPE	Cytopathic effect
CV	Coxsackievirus
CVA9	Coxsackievirus A9
CVB3	Coxsackievirus B3
EGFP	Enhanced green fluorescent protein
EV	Enterovirus
GFP	Green fluorescent protein
GMK	Green monkey kidney
HIV	Human immunodeficiency virus
IF	Immunofluorescence staining
MOI	Multiplicity of Infection
PBS	Phosphate buffered saline
PFU	Plaque-forming unit
pi	Post infection
SARS-CoV-2	Severe acute respiratory syndrome coronavirus 2
sfCherry	Super-folder Cherry
TNT	Tunneling nanotube

1. Introduction

1.1 Enteroviruses

Enteroviruses (EV) are small, non-enveloped viruses classified within the *Picornaviridae* family. Their genetic material is single-stranded, positive-sense RNA, approximately 7.5 kb in length. The genome is densely packed into an icosahedral protein capsid 28 to 30 nm in diameter. The capsid is composed of 60 copies of the four capsid proteins (virus proteins 1-4). VP1, VP2 and VP3 form the outer surface of the capsid while VP4 is located inside. Additionally, there are non-structural proteins that play roles in viral genome replication and interactions with host cells (Laitinen *et al*., 2016).

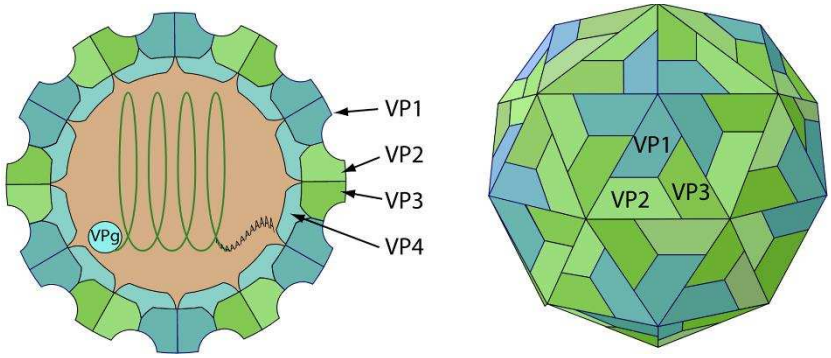

Figure 1: Enterovirus structure. The image was copied from www.viralzone.expasy.org

1.1.1 Overview of Enterovirus classification

Previously, EVs have been classified into four groups based on their antigenic and biological properties: group A coxsackieviruses (CV-As), group B coxsackieviruses (CV-Bs), echoviruses (Es), and polioviruses (PVs) (Oberste *et al*., 2002). However, the molecular characterization of the viral genome has led to a modern classification system that organizes EVs according to their genetic similarities. Table 1 presents the different species of enteroviruses and their types (prepared from Simmonds *et al*., 2020 and www.picornaviridae.com).

Table 1: Enterovirus species and types affecting both human and other animals.

Species	Types	Number of types
Enterovirus A	CVA2, CVA3, CVA4, CVA5, CVA6, CVA7, CVA8, CVA10, CVA12, CVA14, CVA16, EV-A71, EV-A76, EV-A89, EV-A90, EV-A91, EV-A92, EV-A114, EV-A119, EV-A120, EV-A121, EV-A122, EV-A123, EV-A124 and EV-125.	25
Enterovirus B	CVB1, CVB2, CVB3, CVB4, CVB5, CVB6, CVA9, E1, E2, E3, E4, E5 , E6, E7, E9, E11, E12, E13, E14, E15, E16, E17, E18, E19, E20, E21, E24, E25, E26 , E27, E29, E30, E31, E32, E33, EV-B69, EV-B73, EV-B74, EV-B75, EV-B77, EV-B78, EV-B79, EV-B80, EV-B81, EV-B82, EV-B83, EV-B84, EV-B85, EV-B86, EV-B87, EV-B88, EV-B93, EV-B97, EV-B98, EV-B100, EV-B101, EV-B106, EV-B107, EV-B110, EV-B111, EV-B112, EV-B113 and EV-B114.	63
Enterovirus C	PV1, PV2, PV3, CVA1, CVA11, CVA13, CVA17, CVA19, CVA20, CVA21, CVA22, CVA24, EV-C95, EV-C96, EV-C99, EV-C102, EV-C104, EV-C105, EV-C109, EV-C113, EV-C116, EV-C117, and EV-C118.	23
Enterovirus D	EV-D68, EV-D70, EV-D94, EV-D111, and EV-D120	5
Enterovirus E	EV-E1 to EV-E5.	5
Enterovirus F	EV-F1 to EV-F8	8
Enterovirus G	EV-G1 to EV-G28	28
Enterovirus H	SV4, SV28, and SA4	3
Enterovirus I		1
Enterovirus J	EV-J103, EV-J108, EV-J112, EV-J115, EV-J121, and EV-J122	6
Enterovirus K		1
Enterovirus L		1
Rhinovirus A	RV-A1, A2, A7, A8, A9, A10, A11, A12, A13, A15, A16, A18, A19, A20, A21, A22, A23, A24, A25, A28, A29, A30, A31, A32, A33, A34, A36, A38, A39, A40, A41, A43, A45, A46, A47, A49, A50, A51, A53, A54, A55, A56, A57, A58, A59, A60, A61, A62, A63, A64, A65, A66, A67, A68, A71, A73, A74, A75, A76, A77, A78, A80, A81, A82, A85, A88, A89, A90, A94, A96, A100, A101, A102, A103, A104, A105, A106, A107, A108, A109	80
Rhinovirus B	RV-B3, B4, B5, B6, B14, B17, B26, B27, B35, B37, B42, B48, B52, B69, B70, B72, B79, B83, B84, B86, B91, B92, B93, B97, B99, B100, B101, B102, B103, B104, B105 & B106.	32
Rhinovirus C	RV-C1 to RV-C57	57

CV= Coxsackieviruses, PV= Polioviruses, E= Echoviruses, EV= Enterovirus, RV= Rhinovirus.

1.1.2 Clinical Significance and Associated Diseases

Enteroviruses enter the human body through the respiratory or gastroenteric route, triggering an early local inflammatory response and inducing tissue-specific antiviral responses in surrounding cells. From the primary site of infection, the viruses can spread to other tissues, leading to serious consequences for the CNS. Although, poliomyelitis, caused by poliovirus, is the

most extensively researched enterovirus-associated disease, the underlying mechanisms of the disease remain surprisingly poorly understood. (Nomoto *et al*., 2007).

Enteroviruses are among the most common human viruses worldwide, transmitted primarily via the faecal-oral or respiratory route. Symptoms of enterovirus infections include fever, headache, respiratory illness, and sore throat and sometimes mouth sores or rash. The highest incidence of symptomatic infections is observed in children, with 44% occurring in infants under the age of one year (Khetsuriani *et al*., 2006). EV infections exhibit a pronounced seasonal pattern, especially in temperate climates, peaking in summer and fall. In addition to this seasonal variation, individual EV types display unique long-term circulation patterns and can cause sporadic epidemics (Pons-Salort *et al*., 2018). The severity of the infection is influenced by both the type of virus and host-specific factors, such as younger age and male gender, which are associated with a higher susceptibility to more severe disease (Scully *et al.,* 2020). From 2015 to 2017, co-circulation of enterovirus species EV-A, EV-B, and EV-D was documented in 24 European countries (Bubba *et al.,* 2020). The most reported genotypes during this period included CVA6, EV-A71, CVB5, E5–6, E9, E11, E18, E30, and EV-D68. Among these, EV-B was the most common species, accounting for 46% of reported infections, followed by EV-A (19%) and EV-D68 (5%). It is important to note that these reported genotypes largely reflect those causing clinically significant disease, as data predominantly originate from hospital diagnostics. Broader population-based surveillance might uncover additional genotypes circulating asymptomatically in the community.

Enteroviruses (EVs) encompass more than 300 types that can infect humans, causing a wide spectrum of clinical manifestations. Although most EV infections are asymptomatic or mild, they can lead to the common cold, pharyngitis, otitis media, sinusitis, pneumonia, pancreatitis, poliomyelitis, Bornholm disease (epidemic myalgia), aseptic meningitis, myopericarditis,

haemorrhagic conjunctivitis, nonspecific febrile illnesses, herpangina, enteroviral vesicular stomatitis (hand, foot, and mouth disease, HFMD), encephalitis, and acute flaccid paralysis. Mostly EV-A71, coxsackievirus A6, A10, and A16 can cause HFMD. Other enteroviruses, particularly coxsackieviruses B (CVBs), are associated with acute myocarditis and the subsequent development of dilated cardiomyopathy. Several EVs have evolved the ability to invade the nervous system and infect the CNS (Torres *et al*., 2020). This can lead to severe diseases such as aseptic meningitis, encephalitis, acute flaccid paralysis, and acute flaccid myelitis (Yea *et al*., 2020 and Nkosi *et al*., 2021). Paralytic diseases like acute flaccid myelitis are most linked to EV-D68 and EV-A71 infections but have also been associated with rare non-polio EVs, such as EV-C105 and EV-C109 (Barnadas *et al*., 2017). Poliomyelitis, caused by three distinct serotypes of poliovirus, remains the most well-known enteroviral disease. Although almost eradicated, other enteroviruses, such as EV-A71 and EV-D68, have emerged in recent years as significant causes of acute flaccid paralysis, resembling the clinical presentation of poliomyelitis (Chia *et al*., 2014 and Khan 2015).

1.1.3 Enterovirus lifecycle

Life cycle of enteroviruses is presented in Figure 2. The initial step involves receptor-mediated endocytosis. By their attachment to one or multiple cell surface receptors. Depending on the serotype and cell type, enteroviruses use various receptors. For example- PV receptor (PVR, also known as CD155) (Mendelsohn *et al*., 1989) for PV, intercellular adhesion molecule 1 (ICAM-1) (Greve *et al*., 1989) for major groups of rhinoviruses, and coxsackievirus adenovirus receptor (CAR) (Bergelson *et al*., 1997) and co-receptor decay accelerating factor (DAF, also known as CD55) (Bergelson *et al*., 1995) have been identified as the receptors for type B coxsackieviruses (CVB). Despite the discoveries of majority of EV receptors, including the recently identified EV-D68 and coxsackievirus A (CVA)10 receptors (Baggen *et al*., 2016, and Staring *et*

al., 2018), the precise mechanism of EV entry and the exact site of viral genome uncoating remain poorly understood. Following the binding and entry, enteroviruses undergo uncoating to release the viral genome. This process is triggered either by the initial receptor binding or by a pH change that creates a pore in the endosome. Uncoating facilitates the release of the RNA genome from the protective capsid into the cytoplasm or endosome.

Once viral RNA has entered the cytoplasm it is translated by host ribosomes and produce a single large polyprotein, which is proteolytically processed by viral proteinases 2Apro, 3Cpro and 3CDpro into ten proteins (capsid proteins VP0, VP1 and VP3 and non-structural 2A–2C and 3A–3D) and some functional cleavage intermediates.

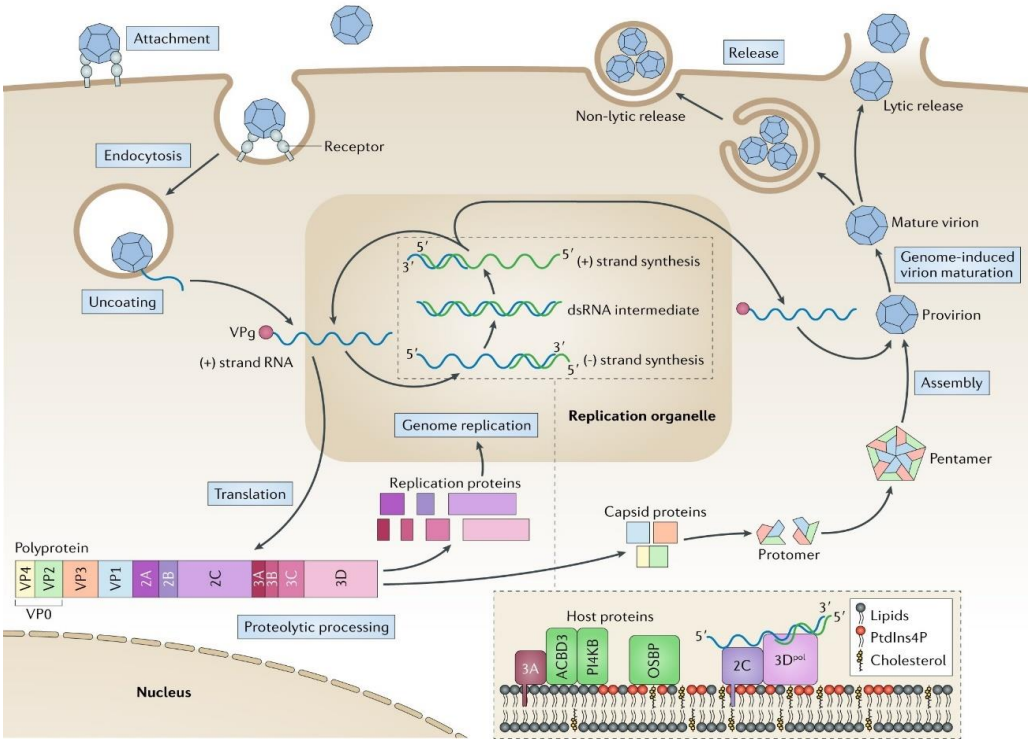

Figure 2: Schematic representation of the enterovirus life cycle. Enteroviruses initiate infection through receptor-mediated endocytosis. Once inside the cell, the virion undergoes uncoating within the endosome, releasing its positive-stranded RNA genome, which is covalently linked to the VPg protein, into the cytoplasm. Host ribosomes translate the viral RNA into a single polyprotein, which is subsequently cleaved by the viral proteases 2Apro and 3Cpro into functional viral proteins.

Following the accumulation of non-structural proteins, including the RNA-dependent RNA polymerase, the viral RNA is replicated. A double-stranded RNA intermediate is formed, with the negative-strand RNA serving as a template for synthesizing additional positive-strand RNAs. These new positive-strand RNAs can either serve as templates for further replication or be packaged as genomes for new virions. Capsid proteins assemble around the positive-strand RNA to form progeny virions. Finally, these virions are released either through lytic cell death or non-lytic pathways involving vesicle-mediated release. Figure was copied from Baggen *et al*., 2018 with permission.

Replication of the enterovirus genome occurs on membrane structures induced by the virus, known as replication organelles (ROs). A viral RNA-dependent-RNA-polymerase enzyme (3Dpol) initiates the synthesis of the negative-stranded copy of the genome making a dsRNA intermediate, which becomes the template to generate new positive-stranded genomes. The structural proteins VP0, VP1 and VP3 are assembled first into protomers and the protomers into pentamers, which form the virus capsid. The newly synthesized positive-stranded genome is packaged into the assembled capsid. After the RNA is packaged into the virion, VP0 is cleaved into VP2 and VP4, which results in mature enterovirus (Pallansch *et al*., 2013 and Baggen *et al*., 2018). Classically, enteroviruses were believed to exit the cell via lytic cell death, releasing progeny virions through cell lysis (Pallansch *et al*., 2013) (Figure 2). However, studies revealed that during infection of PV and a related Picornavirus, hepatitis A virus, progeny virions can acquire host cell membranes and exit the cell in vesicles thus infect new cells through non-lytic pathways (Feng *et al*., 2013 and Bird *et al*., 2014).

1.1.4 Transmission and pathogenesis of enteroviruses

Enteroviruses are primarily transmitted through the faecal-oral route or via respiratory droplets in human-to-human contact, either directly or indirectly through contaminated hands and surfaces. In areas with poor water and sewage infrastructure, transmission via water is likely. Exceptions to the faecal-

oral transmission route include haemorrhagic conjunctivitis caused by enterovirus 70 (EV-B70) and coxsackievirus A24 (CV-A24), which are more likely transmitted through direct eye secretion contact or contaminated swimming pools (Aubry et al., 2012). Hand-foot-mouth disease (HFMD), commonly caused by CV-A16 and EV-A71, can also be transmitted through vesicular fluids. Enteroviruses can spread effectively at public events, schools, and sports team activities, sometimes causing outbreaks (Pallansch, 2013).

Almost all enteroviruses replicate in the oral-pharyngeal mucosa or tonsils before entering the gastrointestinal tract or bloodstream in a viremic state. Enteroviruses are acid-stable, allowing them to pass through the intestinal tract to the faeces and cause secondary infections at other sites (Pallansch, 2013). They can enter the central nervous system via axons or by crossing the blood-brain barrier (BBB), a process studied in poliovirus using mouse models (Ren and Racaniello, 1992; Aubry *et al*., 2012). Additionally, some symptoms, such as exanthema and cardiac disease, can result from the host immune response (Palacios and Oberste, 2005).

1.1.5 Vaccines against enteroviruses

Significant progress has been made in developing vaccines against enteroviruses, including polioviruses, coxsackieviruses, and enterovirus 71 (EV71) (Pallansch 2006). The inactivated polio vaccine (IPV) and oral polio vaccine (OPV) had impact in nearly eradicating poliomyelitis globally, though concerns about vaccine-derived poliovirus have shifted focus to IPV. For EV71 (Zhu *et al.,* 2014), inactivated vaccines licensed in China have shown high efficacy in preventing hand, foot, and mouth disease. Additionally, virus-like particle (VLP) vaccines, which closely resemble the structure of the native virus, are promising for EV71 and coxsackievirus A16. (*Chong et al.,* 2015). Advances in mRNA and DNA vaccine technologies, as seen with SARS-CoV-2 vaccines, are now being applied to enteroviruses, offering rapid development and scalable production (Ilyichev *et al*., 2020). Furthermore, novel adjuvants and

combination vaccines are being investigated to boost immune responses and provide broader protection. These advancements are critical for reducing the global burden of enterovirus-related diseases.

1.2 Modes of cell-to-cell virus spread

Viruses are small obligate intracellular parasites that rely on host cells for the complex metabolic and biosynthetic machinery necessary for their replication. For a complete life cycle, virus need to target non-infected cells to initiate new infections. Most non-enveloped, such as enteroviruses, kill the host cells and release particles into the extracellular space. However, some have developed methods to transfer viral particles or components directly between cells, without the requirement for release into the extracellular environment (Cifuentes-Munoz *et al*., 2020).

1.2.1 Cell-free spreading

Releasing the viral particles into the extracellular space, target and subsequent re-entry into another host cell for infection is the most common and best described mechanisms of virus spread. This mode of spreading is important for transmission between distant cells and hosts. To initiate an infectious cycle, virions must interact with surface molecules of new target cells, including receptors, co-receptors, and attachment factors. Viral particles can be released through various mechanisms, for example: (i) cell lysis induced by viral proteins, common in non-enveloped viruses like reoviruses, caliciviruses, adenoviruses, and picornaviruses (Nieva *et al*., 2012; Giorda and Hebert, 2013); (ii) budding directly from the plasma membrane, where virions acquire an envelope, seen in viruses like human immunodeficiency virus 1 (HIV-1), influenza, paramyxoviruses, and pneumoviruses (Lorizate and Krausslich, 2011; Weissenhorn *et al*., 2013); (iii) viral particles or components are packaged into extracellular vesicles such as exosomes and micro-vesicles, which are then secreted into the extracellular space. Such observations were made for rotavirus

(Santiana *et al*., 2018), CVB3 and rhinovirus (Chen *et al*., 2015). While cell-free transmission allows movement over long distances, it is often very inefficient. In addition, it is subject to several barriers in the host organism or target cell can hinder effective transmission through the cell-free mode.

1.2.2 Direct cell to cell contact spreading

Direct cell-cell contact is a highly efficient method for viral spread, overcoming intrinsic immunity and other entry-related barriers, delivering genomic cargo directly to target cells (Cifuentes-Muñoz *et al*., 2018). This mode of spread involves the transfer of viral particles directly from an infected cell to a neighbouring uninfected cell through various mechanisms.

Syncytia are cellular structures formed through the process of multiple cell fusions, resulting in multinuclear cells. The process of viral-induced syncytia formation begins with the virus entering a host cell and expressing its proteins, including fusion proteins (Figure 3). These fusion proteins are then transported to the infected cell's membrane. Upon activation, often triggered by receptor binding or other factors, the fusion proteins undergo conformational changes. The activated proteins on the infected cell bind to receptors on adjacent cells, causing their membranes to merge. As more cells fuse, a large multinucleated cell, or syncytium, is formed, facilitating direct viral spread. Syncytia formation for virus spread is used by several viruses including coronavirus, herpesviruses, HIV, and respiratory syncytial virus (Cole and Grose, 2003; Buchrieser *et al.,* 2020; Leroy *et al*., 2020). This virus-induced cell fusion facilitates in the transfer of viral genomes to adjacent cells.

Virological synapses are specialized contact points where viral particles are transferred from an infected cell to a target cell. These synapses involve the reorganization of the cytoskeleton and the clustering of receptors and adhesion molecules at the contact site, facilitating efficient viral transfer that has been shown to be used by retroviruses (Dupont and Sattentau, 2020).

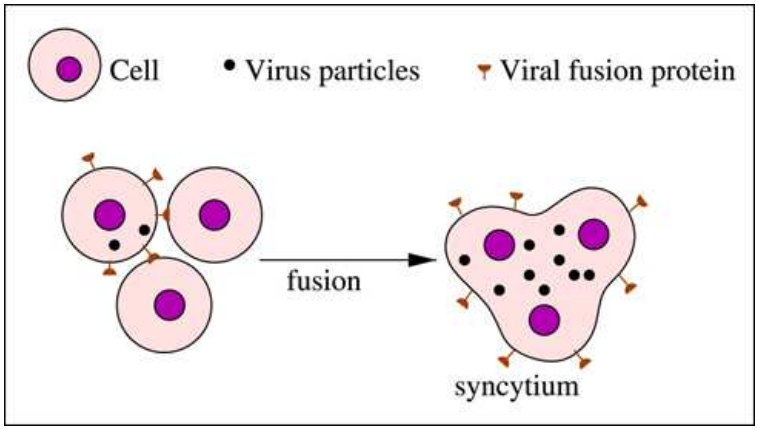

Figure 3: Viral-induced syncytium formation. A syncytium is a multinucleated cell structure formed by the fusion of individual cells; a process often induced by specific viruses. Viral-induced syncytium formation occurs when viral fusion proteins on the surface of infected cells mediate the merging of neighbouring cell membranes. This phenomenon is common in infections caused by certain paramyxoviruses (e.g., measles virus), retroviruses (e.g., HIV), and herpesviruses (e.g., HSV-1). This image was copied from Alzahrani *et al*., 2020 with permission.

Some viruses exploit actin-based structures like nanotubes and filopodia to move between cells. These structures create direct cytoplasmic connections induced by actin polymerization underneath the plasma membrane, allowing the virus to travel from one cell to another without exposure to the extracellular environment. These structures are different from tunneling nanotubes (TNTs) which are thin, elongated membrane-bound structures, connect two distant cells and allow the transfer of material including virus, organelles, ions, proteins and miRNAs (Rustom *et al*., 2004).

1.3 Tunneling Nanotubes (TNTs): An Overview

1.3.1 Discovery and Definition

Researchers discovered a new form of cell-to-cell communication and named these Tunneling nanotubes (Rustom *et al*., 2004). TNTs (Figure 4) are thin membranous protrusions that connect cells directly to each other and are not a result of cell division. They have a diameter between 50 and 700 nm, length

between 20 and 100 µm. They contain actin, are open-ended, do not adhere to the substratum and connect the cells using continuous plasma membrane.

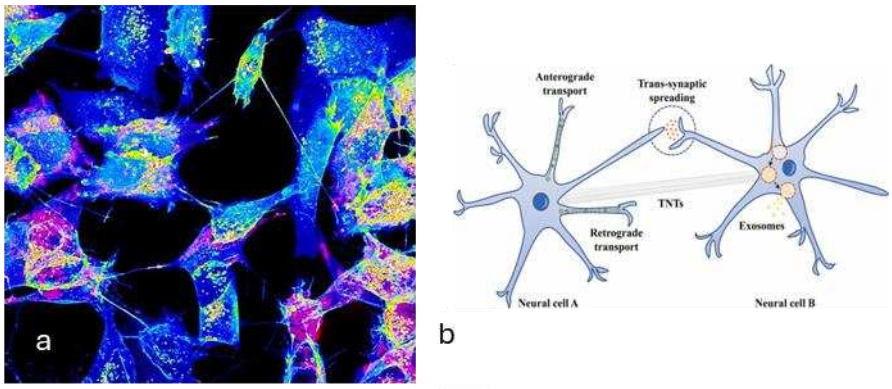

Figure 4: Cell-to-cell connections by Tunneling nanotubes (TNTs). (a) An image of epithelial cells connected by TNTs. This image was copied from Institut Pasteur web page (https://www.pasteur.fr/en/home/research-journal/news/when-structure-tunneling-nanotubes-tnts-challenges-very-concept-cell, Sartori-Rupp *et al.* 2019). (b) An illustration of human neuronal cells connected by TNTs, which are different from synaptic connections, also shown in the image (Wang *et al.*, 2021). Images were copied with permission.

Since their discovery, TNTs are reported among various cell types *in vitro*, for example in endothelial, neuronal, epithelial, muscle, mesenchymal, and immune cells (Yamashita *et al*., 2018). The most distinctive feature of TNTs is their ability to transfer a diverse range of cargoes between cells. These include small molecules like-calcium ions, nucleic acids, and proteins, as well as some larger cellular organelles such as vesicles, lysosomes, mitochondria, and autophagosomes (Abounit *et al*., 2012). A functional cellular network is formed with the connection of multiple cells by TNTs (Ariazi *et al*., 2017).

1.3.2 Structural and Functional Characteristics

TNTs can be distinguished from other protrusions found in cells, such as cytonemes, cilia, or filopodia. The morphology of TNTs may differ in length, and thickness as well as the composition of the cytoskeleton (Rustom *et al*., 2004), which may contain actin, and microtubules (Figure 5). These

microtubules containing protrusions are thicker than typical TNTs and have closed ends (Figure 5c). Some of the cellular connections are observed to contain only actin and others contain both actin and microtubules (Souriant *et al.*, 2019).

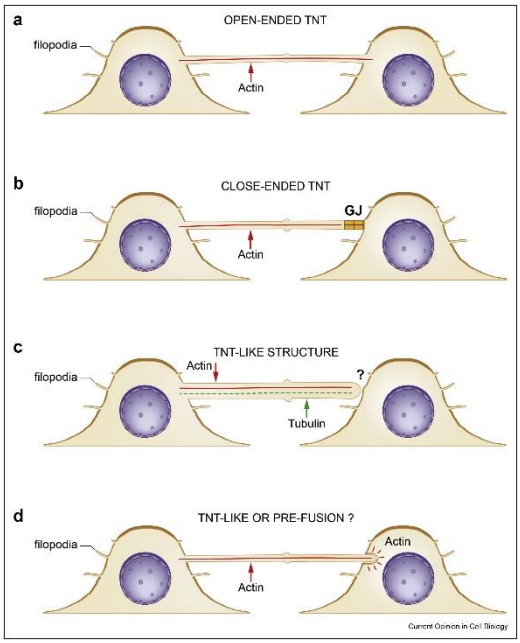

Figure 5: Schematic representation of different TNTs and TNT-like protrusions observed *in vitro*. (a) Open-ended TNTs containing filamentous actin. (b) Closed-ended TNTs containing actin and a Gap Junction placed at one end. Electrical signals and small molecules can transfer through them. (c) Closed-ended TNT-Like structures containing both actin filaments and microtubules. (d) Closed-ended TNT-like structures pushing into the connecting cell or prefusion event of a standard TNT. Picture copied from Zurzolo *et al.*, 2021 with permission.

According to the research of Hanna *et al.*, 2019, the formation mechanism of TNTs involves an actin-driven process. It starts with the activation of the actin nucleation complex, leading to the subtle elongation of extensions through actin polymerization in a specific orientation. Subsequently, membrane fusion occurs in the presence of various fusion molecules and adhesion proteins. During this phase, the tips of TNTs are mostly dynamic and transient, making them rarely visible. Additionally, changes in actin filament dynamics can generate diverse cellular protrusions, facilitating complex intercellular communication (Gerdes *et al.*, 2013).

TNTs are vulnerable to both internal and external interventions. Their typical structure and functionality can be compromised by shear stress and extended light exposure, particularly during their formation (Koyanagi *et al*., 2005). Additionally, the creation of these membranous nanotubes can be inhibited in low cell densities due to the increased intercellular distance.

Although TNTs have been found in normal physiological conditions, their formation may be triggered with various stress stimuli, including inflammation, serum starvation, oxidative stress, UV radiation, hyperglycaemic conditions, hypoxia, low pH, etc (Wang *et al*., 2015). TNT formation might serve as a stress response mechanism, aiding the transfer of biomolecules and energy between damaged and healthy cells. TNT-mediated intercellular communication contributes to the development and progression of various pathologies, such as neurodegenerative diseases, cancer, and infectious diseases.

1.3.3 Mechanisms of TNT Facilitation in Virus Spread

Viral infections induce the creation of TNTs or TNT-like structures utilizing both viral and host proteins, which are then used to effectively spread infection and transmit molecular information to adjacent cells. TNTs allows a faster route of virus spread by creating a direct pathway for viral particles, proteins, and other cellular components to move between cells, avoiding the extracellular environment and making the process more efficient. Intracellular viral spread via TNTs protects against immune detection of host defence system and allows infectious particles to move from infected to vulnerable cells, even otherwise non-permissive cells (Tiwari *et al*., 2021; Pepe *et al*., 2022). Several viruses have been seen to induce TNTs and move through them to non-infected cells, these are severe acute respiratory syndrome coronavirus 2 (SARS-CoV-2), herpesvirus, Influenza A and HIV.

Besides causing mild respiratory issues to severe pneumonia, SARS-CoV-2 infection can lead to neurological complications by invading the central nervous

system (CNS). However, the mechanism of SARS-CoV-2 spread in the human brain remains unclear, given that ACE2 receptor levels are minimal in most parts of brain, preventing entry through receptor-mediated endocytosis. (Chen *et al*., 2020). In 2022, scientists showed that SARS-CoV-2 can spread from infected cells to non-permissive neuronal cells *in vitro* via direct cell-to-cell contact forming TNTs (Pepe *et al*., 2022).

A recent study using fluorescently labelled viral proteins and time-lapse confocal microscopy demonstrated that herpesviruses gain protective advantages by traveling through TNTs, which allows them to evade detection by the immune system. Even in the presence of neutralizing antibodies, alpha-herpesvirus BoHV-1 can transmit viral particles and cellular organelles along TNTs formed by bovine primary fibroblasts and oropharynx cells (Panasiuk *et al*., 2018).

Roberts *et al*., 2015 observed Influenza A virus (IAV) infected cells to form intercellular connections rich in F-actin. Additionally, they found that the influenza virus genome is present in TNTs connecting infected and uninfected cells. Furthermore, Kumar *et al*., 2017 showed that IAV genome and proteins can be transferred through TNTs, and this leads to virus propagation. They used hemagglutination-inhibiting antibodies and the neuraminidase inhibitor Oseltamivir to block virus extracellular transfer through growth medium. Human macrophages were initially observed to increase TNT production upon HIV infection, and this was associated with viral replication. While HIV induces TNT formation in macrophages, there is no increase in TNT production in HIV-infected T cells. Nevertheless, the virus utilizes TNTs to travel between and infect T cells (Sowinski *et al*., 2008, Eugenin *et al*., 2009). Formation of TNTs in blood monocyte-derived macrophages involves the HIV accessory protein Nef and the cellular protein M-Sec (Hashimoto *et al*., 2016). Interestingly, recent research has also demonstrated that co-infection with HIV and Mycobacterium tuberculosis stimulates the formation of TNTs (Souriant *et al*., 2019).

1.3.4 Therapeutic Opportunities and Challenges

In recent years, several studies have highlighted TNTs as a potential target for treating tissue injury, overcoming tumour drug resistance, and combating infections. Therefore, research has started exploring approaches to inhibit TNT formation for treating diseases. Conversely, there is also interest in protecting or promoting TNT formation, as it may facilitate the delivery of "defensive tools" to repair injured normal cells (Vignais *et al*., 2017) and serve as a natural mechanism for tissue self-repair during pathological conditions.

TNTs could provide a novel and highly specific method for intercellular delivery of bio-macromolecular drugs, such as polypeptides, proteins, antibodies, glycans, and nucleic acids, as well as drug carriers. Typically, this mechanism depends on slow diffusion and often struggles to effectively reach target cells (Dewhirst *et al*., 2017). Doxorubicin, a chemotherapeutic drug has been observed to transfer in pancreatic, ovarian, and lung cancer cells, suggesting this TNT networks may be efficiently employed to redistribute antitumor drugs among connected tumour cells (Omsland *et al*., 2017; Desir *et al*., 2018).

Studying TNTs *in vivo* is challenging due to the lack of well-defined molecular markers and mechanisms for identification. Their precise role in molecule transfer during homeostasis or disease remains mostly unclear. The three-dimensional structure of TNTs within complex and unstable tissue environments necessitates the use of high-resolution imaging techniques. Variations in morphology, the lack of specific molecular markers for identification, and limitations in imaging resolution continue to pose challenges in TNT research.

1.4 Split Fluorescent Protein technology

Fluorescent molecules are essential and versatile tools in bio-analytical research, enabling the tracking of biological molecules and monitoring dynamic processes in living cells.

Green Fluorescent Protein (GFP) facilitates high-resolution imaging and quantification of intricate cellular events, it is widely employed in life sciences and biomedical research. GFP, discovered by 2008 Nobel laureate Osamu Shimomura, was initially identified while studying the bioluminescent system in the jellyfish *Aequorea victoria* (Shimomura *et al*., 1962). His team successfully extracted and purified "green protein" from *A. victoria* (Johnson *et al*., 1962). Although the crystal structure of GFP (Morise *et al*., 1974) and its X-ray diffraction pattern (Perozzo *et al*., 1988) have been available since 1974 and 1988 respectively, its detailed structure remained unknown until 1996. That year, Roger Tsien, a 2008 Nobel laureate in Chemistry, and his team revealed the structure of GFP (Ormö *et al*., 1996).

The green fluorescent protein (GFP) is a 27 kDa polypeptide, comprising 238 amino acids. Wild-type GFP has a β-barrel structure consisting of 11 β-strands, enveloping an α-helix that houses the chromophore [4-(p-hydroxybenzylidene) imidazolidin-5-one (HBI)] derived from Ser-65, Tyr-66, and Gly-67. Proper GFP folding is crucial for its fluorescence (Tsien, 1998), as the β-barrel shields the chromophore from fluorescent quenchers like water, triplet oxygen, and photoisomerization within the protein core.

Split GFP technology involves dividing the green fluorescent protein (GFP) into two non-fluorescent fragments: a larger GFP1-10 fragment and a smaller GFP11 fragment. These fragments are individually non-fluorescent but can reassemble into a functional, fluorescent GFP when they are brought together. The GFP1-10 fragment, containing the three residues forming the GFP chromophore is nonfluorescent, requires the conserved E222 residue on GFP11 for chromophore

maturation. The reconstituted GFP becomes fluorescent after the chromophore maturation reaction is completed. The mechanism by which split GFP technology operates is illustrated in Figure 6. This technology enables researchers to visualize and quantify various molecular events within living cells, i.e., visualization of protein subcellular localization, cell-cell contact detection, etc. (Kamiyama *et al*., 2016).

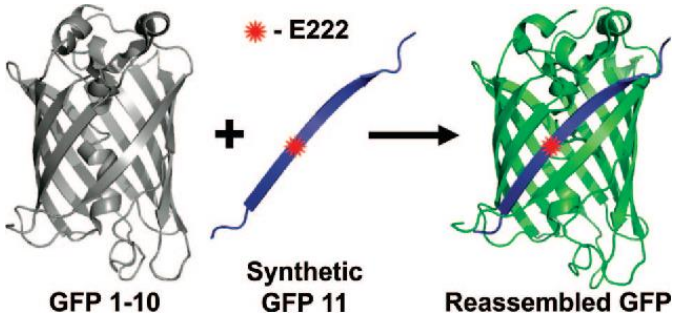

Figure 6: Illustration of the split GFP technology. The GFP 1-10 fragments (which includes residues 65-67 that form the chromophore) and a synthetic 16 amino acid segment GFP 11 reassemble to form the green fluorescing complete GFP. The red star indicates residue E222 on GFP 11. The image was copied from Kent *et al*., 2008 with permission.

A monomeric red fluorescent protein (mRFPs) mCherry is a member of the so called mFruits family having several fluorescent proteins of different colour. The mCherry was derived from DsRed of *Discosoma* sea anemones (Shaner *et al*., 2004) and its structure resembles the GFP consisting of 11 β-strands. Starting with the monomeric fluorescent protein mCherry (Shu *et al*., 2006), a super folder variant, optimized for folding efficiency, named sfCherry was created by directed evolution. Similar to the split GFP assays, a split sfCherry$_{1–10/11}$ system was derived from the super-folder Cherry (Nguyen *et al*., 2013; Kamiyama *et al*., 2016).

1.5 Aims of the study

Enteroviruses typically exit the host cell through cell lysis by disrupting the cell membrane. However, previous research has indicated that some viruses use tunneling nanotubes or similar structures for cell-to-cell spread. The discovery of cell-to-cell movement for enterovirus spread would be a novel finding. Furthermore, it would be the first human non-enveloped virus discovered to utilize this route of spread. This finding might explain some features of enterovirus infections of the brain or pancreas. It is crucial to understand virus biology when designing antiviral strategies. The aim of our study was to:

1. To optimize methodology for the study, such as fluorescent staining and transfection reagents for the cell lines used.
2. To employ the split GFP technology as a tool to visualize cell connections.
3. To confirm that enterovirus infection induces TNTs.
4. To investigate the possible cell-to-cell movement of Coxsackievirus A9 and Coxsackievirus B3 through TNTs.

2. Materials and Methods

2.1 Materials

Cells and viruses: Cell lines used in this study were all isolated from the kidney of the African green monkey (*Cercopithecus aethiops*): GMK (collected from Dept. Of Biomedicine cell bank), Vero (ATCC® CCL8) and Vero E6 (ATCC No. CRL-1586).

Enteroviruses used were coxsackievirus B3 (CVB3) strain Nancy (VR-30) and coxsackievirus A9 (CVA9) strain Griggs (VR-1311). These were originally acquired from American Type Culture Collection (ATCC).

Antibodies and other staining reagents: Antibodies used in this study were to recognize virus protein and double stranded RNA (dsRNA), which are the indicator of active virus replication and are not present in uninfected cells. The antibodies to detect virus protein were: rabbit polyclonal anti-CVB3 (in house), rat anti-EV (3A6) (in house, a kind gift of Professor Vesa Hytönen, Tampere University), mouse monoclonal anti-EV (5D8/1) (DAKO), mouse monoclonal anti-EV (9D5) (clone 3361, Light Diagnostics). The mouse monoclonal anti-dsRNA (mabJ2) (Cell signaling technology) was used to detect dsRNA. Secondary antibodies used were: goat anti-mouse (green, Alexa Fluor 488 A11001), donkey anti-rabbit (red, Alexa-Fluor 594 A21207), goat anti-rabbit (green, Alexa Fluor 488 A11008), goat anti-rat (green, Alexa Fluor 488 A11006).

In addition, several small molecules were used to stain nucleus (DAPI, Thermo Fisher Scientific), actin filaments (Phalloidin, Alexa Fluor™ Plus 647) and the cellular plasma membrane (PlasMem Bright Red, DOJINDO P505-10). All the antibodies and staining reagents were optimized first for the cell line, viruses, and experiments.

Plasmids: Bacterial plasmids containing split super-folder cherry and split green fluorescent protein were obtained from Addgene (www.addgene.org). The

control enhanced green fluorescent protein (EGFP) expressing plasmid was a kind gift from Dr. Jukka Alinikula, (Adjunct Professor, Institute of Biomedicine, University of Turku). All plasmids express the proteins in Mammalian cells and are described in studies by Kamiyama *et al.,* (2016) and Cieri *et al.,* (2018). Plasmid pcDNA3.1-GFP1-10 (Addgene Plasmid 70219) expresses GFP1-10, plasmid SacI ML GFP Strand 11 Short (Addgene Plasmid 164121) expresses GFP11, plasmid pcDNA3.1-sfCherry1-10 (Addgene Plasmid 70222) expresses sfCherry1-10 and plasmid pEGFP-sfCherry11x4-ß-actin (Addgene Plasmid 70220) expresses sfCherry11 coupled to ß-actin.

Transfection reagents: For the efficient transfection of split GFP and split sfCherry several transfection reagents were tested. These were Lipofectamine-2000, Lipofectamine-3000 and Turbofect (Invitrogen, Thermo Fisher Scientific), TransIT Lt1 (Mirus Bio), JetOPTIMUS (Polyplus), Transfectin (Bio Rad) and K2-transfection System (Biontex).

2.2 Culturing and maintenance of the cell lines

The cells were cultured in growth media- Dulbecco's Modified Eagle's Medium (DMEM) (Lonza Biowhittaker) supplemented with 10% (v/v) Fetal Bovine Serum (FBS, Gibco), 1 % Penicillin/Streptomycin (Lonza Biowhittaker) at 37°C and 5% CO_2. Frozen stock cells were collected from the cell bank and cultured in a tissue culture flask (25 cm^2). Next day, the media was changed to remove the remaining DMSO used for freezing of cells. For splitting, the culture flask (25 cm^2) with a confluent monolayer of cells was washed with 10 mL Phosphate Buffered Saline (PBS, Gibco), overlaid with 500 µL trypsin (0.25% solution, Gibco) and incubated at 37°C for 5 minutes. The flasks were checked using a light microscope to confirm the detachment of cells from the surface and were resuspended in 4 mL growth media to stop further trypsinization (This procedure was used for further experiments, where cells were needed). The cells were passaged into a new tissue culture flask (75 cm^2) and incubated at

37°C with 5% CO_2. The cells were split once a week, 1:4 into new culture flasks with fresh media.

Cells were counted using an automated cell counter (TC20, Bio-Rad Laboratories, Inc). An equal amount (10 µL) of detached cells and ready to use Trypan blue solution (Bio-Rad Laboratories, Inc) were mixed and loaded onto a chamber slide and measured with the cell counter.

2.3 Virus stock preparation

A new CVB3 virus stock was prepared for this study. A vial of frozen CVB3 stock was thawed inside a laminar flow cabinet. Previously prepared 75 cm^2 culture flasks containing monolayers of GMK, Vero, and Vero E6 cells were each inoculated with 1 mL of viral stock diluted in 3 mL infection media (DMEM supplemented with 2% FBS, Penicillin/Streptomycin and Glutamax). The culture flasks were moved to a CO_2 incubator at 37°C for 1h. Virus inoculates were discarded, cells were rinsed with 5 mL PBS, 20 mL of fresh infection media was added to the cell culture flask and incubated at 37°C with 5% CO_2 for 24-48h. Infected cells were followed using a light microscope for the formation of a cytopathic effect (CPE).

When the CPE reached about 80%, the flask was frozen at -20°C. For the final preparation of virus stock, the flasks underwent three freeze-thaw-cycles to break open the remaining intact cells. The cell debris was centrifuged at 3000 rpm for 5-10 min. Supernatants were moved to cryotubes and labelled properly with virus name, harvest date, used cell line, passage and stored in -80°C.

2.4 Determination of virus amount

Virus quantification is crucial to determine the Multiplicity of Infection (MOI), which is the ratio of virus particles to target cells. Two cell-based assays were followed:

2.4.1 Plaque assay

Plaque assay determines the number of plaque forming units (PFU) in a virus sample, where one plaque equals one infective virus. 6-well plates were prepared for two virus strains using three cell lines with target cell count: 1-1.5 x 10^6 cells/well in 2 mL of growth media. The plates were incubated at 37°C with 5% CO_2 for 1-2 days to grow cells to a confluent monolayer. Serial 10-fold dilutions were made of the stock virus into infection media as presented in figure 7.

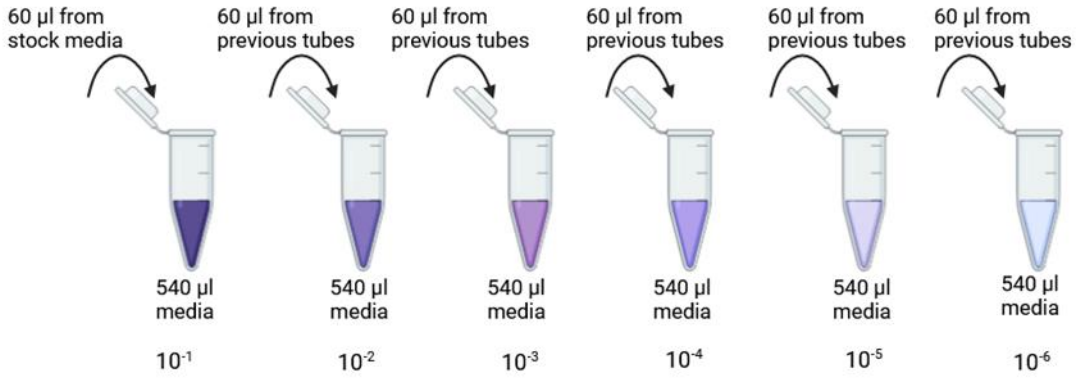

Figure 7: The preparation of serial dilution made in Eppendorf tubes. The image was prepared with BioRender.

The previously prepared 6-well plates were infected with 500 µL serial virus dilutions, 10^{-2} to 10^{-6}, after discarding the old media. One well was kept as a control and 500 µL of infection media (without virus) was added to it. The plates were incubated at 37°C with 5% CO_2 for 2h, gently tilting the plates about every 15 minutes during the first hour. The medium was changed to a 1.2% Avicell solution in infection medium to prevent the virus infection from spreading through the medium and again incubated at 37°C with 5% CO_2 for 24h. To fix the cells, the Avicell solution was changed to 500 µL 4% formaldehyde per well and incubated in a biosafety cabinet (laminar) for 30 min. Cells were stained with Crystal violet and the number of plaques were counted. The pfu was calculated for the original stock virus solution.

2.4.2 TCID50 endpoint assay

Virus titre was also determined by 50% Tissue Culture Infectious Dose (TCID50) in 96-well plates. Virus stocks of both CVA9 and CVB3, were serially diluted 10-fold in 96-well plates (Figure 8) using infection media, each column with a different virus dilution (first dilution into wells A1-H1, second dilution A2-H2 etc.). The last column (A12-H12) was the control with no virus, only infection media. GMK, Vero, and Vero E6 cell suspensions ($5x10^4$ cells/50 µL) were prepared in infection media and 50 µL was added to each well already containing the virus dilutions and incubated at 37°C with 5% CO_2 for 2-3 days.

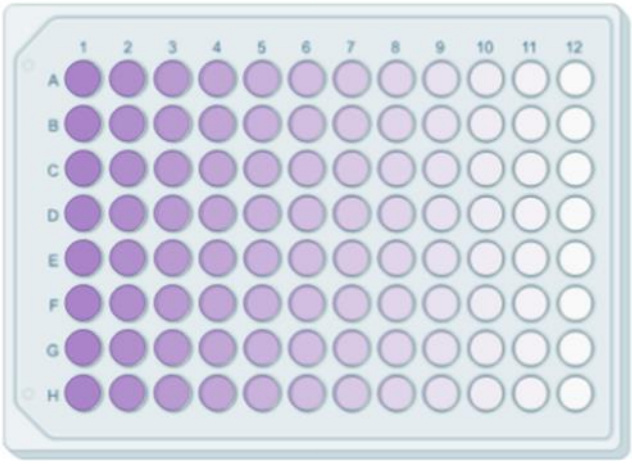

Figure 8: Preparation of serial dilution made in 96-well plate. The image was prepared with BioRender.

The CPE was observed under a light microscope and scored. When the CPE did not increase anymore in the most diluted virus wells, cells were fixed by adding 150 µL 8% formaldehyde to wells without discarding the old media, and incubated in a biosafety cabinet (laminar) for 30 min. After that, the liquid was discarded, and cells were stained with Crystal violet. The virus titre was calculated according to Read and Muench method and expressed in $TCID_{50}$/ml for the original stock virus (Reed and Muench, 1938).

2.5 Infection and Neutralization experiments

All the experiments were continued using GMK cells. A confluent monolayer of cells was detached from cell culture flasks. Cells were then diluted to $3x10^4$ and $4x10^4$ cells per 50 µL in infection media and added to wells of black 96-well plates. Several dilutions of CVA9 and CVB3 viruses were prepared in Eppendorf tubes, based on the MOI established and 100 µL of virus dilution was added to the cells in different wells. To the control cells, 100 µL of infection media was added. The plates were incubated for 24h after which the cells were fixed with 150 µL 4% formaldehyde and stored for immunofluorescence assays. An overview of the infection experiment is represented in figure 9.

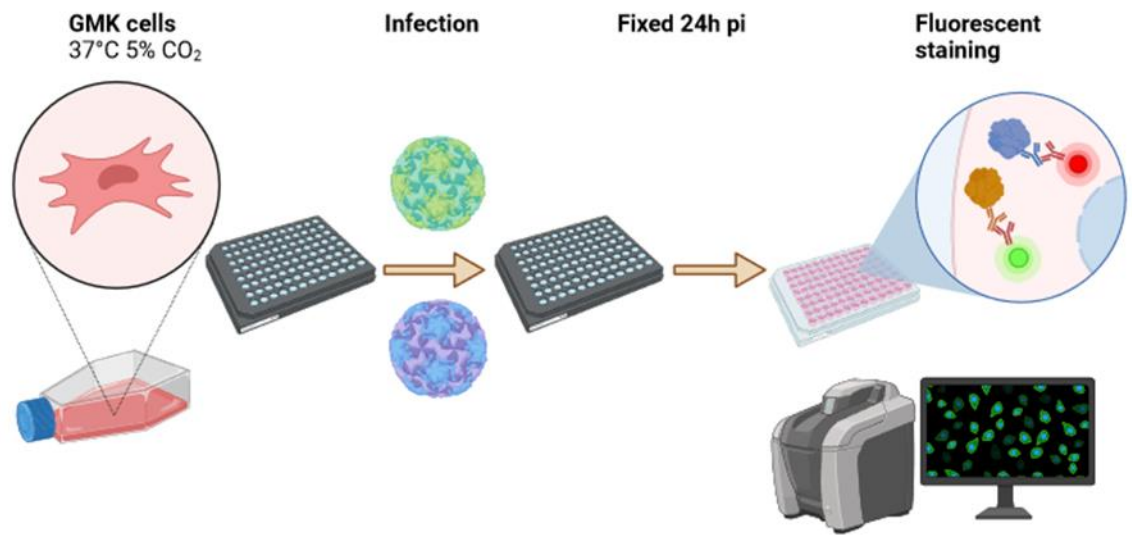

Figure 9: Generalized representation of the overall experiment workflow. Image was prepared with BioRender.

For neutralization experiments, CVB3 and the neutralizing antibody Rabbit polyclonal anti-CVB3, was added in 100 µL infection media with different concentration (Table 2, in the result section). In a 96-well plate, they were mixed and incubated for 1.5h at 37°C. Cells were then diluted to $4x10^4$ cells per 50 µL in infection media and pipetted on top of the virus and antibody mixtures. The plate was then kept in the incubator and CPE was followed daily for several days.

2.6 Immunofluorescence (IF) staining

The infected and fixed black 96-well plates were washed several times with 100 µL PBS and permeabilized with 0.2% Triton-X 100 in PBS at RT for 15 min. The wells were washed 3x5 min with 100 µL PBS. Primary antibody diluted into 3% BSA in PBS was added in a volume of 60 µL and incubated for 1h at RT on a rotary shaker. Primary antibodies are listed with the concentration studied and optimal concentrations in Table 2, results section. After another wash with PBS, 60 µL of labelled secondary antibody was added (1:400, diluted into 3% BSA in PBS). Secondary antibodies were selected based on their appropriate labels and compatibility with the specific primary antibodies used. The secondary antibody solution was incubated for 1h at RT in a dark chamber.

For staining actin filaments or plasma membranes, Phalloidin (Concentrations mentioned in the result section, Table 2) or PlasMem Bright Red (diluted 1:1000 in 3% BSA in PBS) was applied to the secondary antibody solution. After washing with PBS, the nuclei were stained with DAPI (1:2000) diluted in 3% BSA in PBS for 5-10 mins in dark. After a final wash, 100 µL PBS was added to the wells to keep them moist and the plate was stored at +4°C in dark. The stained cells were visualized with an EVOS® FL Auto microscope (Thermo Fisher Scientific) using 3 fluorescence channels, with different magnification and documented accordingly.

2.7 Split GFP workflow

2.7.1 Plasmids purification

Plasmids were obtained in live bacteria as agar stabs. Bacteria were cultured first on agar plates (10gm Agar and 16gm LB in 1L) and then grown in LB media (10 mL) supplemented with the appropriate antibiotic (ampicillin or kanamycin). Bacterial pellets were subjected to plasmid DNA extraction using the QIAprep Spin Miniprep Kit (QIAGEN), following the manufacturer's instructions. DNA concentration was measured using NanoDrop.

2.7.2 Transfection

Initial optimizations were conducted in 24-well plates. Different transfection reagents were experimented with to assess transfection efficiency in GMK cells. Cells were seeded at a density of $2x10^5$ cells per well in growth media one day prior to transfection to achieve 70–90% confluency. EGFP was then transfected into the cells using various transfection reagents at different concentrations, following the manufacturer's protocol (presented in Table 3 in the results section). Following transfection, cells were incubated for 48h. Transfection efficiency was determined by GFP fluorescence of transfected cells using the EVOS® FL Auto microscope at both 24- and 48h post-transfection.

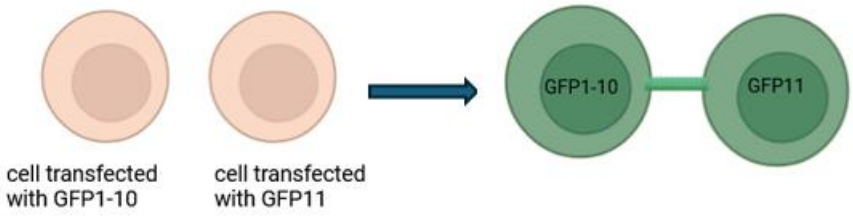

Figure 10: Overview of Split GFP workflow. Cells were transfected with split GFP plasmids, resulting in each cell containing one segment of the GFP DNA upon successful transfection. Individually, these fragments are non-fluorescent and incapable of producing fluorescence until these cells form direct connections that allow the fragments to come into close enough proximity to reassemble. This interaction facilitates the engagement of the two target proteins, allowing them to reassemble into a functional GFP (shown in figure 6, introduction), thereby emitting green fluorescence. An identical workflow is employed for experiments utilizing split sfCherry.

After the optimization, the most efficient transfection reagents were selected with optimum concentration to evaluate the functionality of split GFP technology for visualizing cellular connections in GMK cells. Transfection experiments were designed with the aim of confirming these connections as open-ended and allowing virus transmission through them. For this purpose,

split GFP technology offers a valuable approach to visualize and verify such open cellular interactions. To allow for distinct colour combinations with antibodies in IF staining, both split GFP, which emits green light, and split sfCherry, which emits red light, were used. These two proteins are structurally similar, making them suitable for use in this technology. The mechanism underlying the functionality of split GFP technology is illustrated in Figure 10.

Transfection of both GFP or sfCherry plasmid segment together: These experiments were done in 24-well plates. The GMK cells were seeded in growth media having $2x10^5$ cells per wells on the previous day to reach 70–90% confluency. Selected transfection reagents were used according to the provided protocol. Both GFP1-10 and GFP11 plasmids were added to the same wells, with 0.25 ng or 0.5 ng of each. EGFP was used as a control to confirm successful transfection. Transfected cells were then incubated for 48h. After 24h and 48h, fluorescence of transfected cells was visualized and captured using EVOS® FL Auto microscope. The same protocol was followed to study the transfection of cells with sfCherry1-10 and sfCherry11.

Transfection of GFP or sfCherry plasmid segments separately and co-culture: Following selection of the optimal transfection reagents, split GFP and split sfCherry plasmids were transfected separately into GMK cells. Cells were first seeded onto 24-well plates at a density of $2x10^5$ cells per well to reach 70–90% confluency. The next day, cells were transfected in separate wells with each fragment of split GFP (one well with GFP1-10 and another with GFP11) and incubated at 37°C with 5% CO_2 for 24h. Cells expressing either GFP1-10 or GFP11 were then detached with trypsin, combined in equal amounts and transferred onto black 96-well plates, at a density of $4x10^4$ cells per well. This procedure was repeated with split sfCherry plasmids. To enhance TNT formation, cells transfected with split GFP or split sfCherry fragments were subsequently infected with both CVA9 and CVB3. Appropriate controls (plain cells, uninfected transfected cells) were treated as the experiment cells without

some of the used reagent. Cells were incubated at 37°C with 5% CO_2 for the duration of the experiment.

In a modified setting, neutralizing antibodies were added to half of the infected cells. After 4h of infection of cells with CVB3, when the virus had not completed its replication cycle and started spreading, the culture medium was replaced with the new infection media containing Rabbit polyclonal anti-CVB3 to serve as a neutralizing antibody. This prevents the virus from being released from lysed cells, and spreading through the medium, that's why viral transmission is restricted solely to cell-to-cell contacts. Cells were incubated at 37°C with 5% CO_2 for the duration of the experiment.

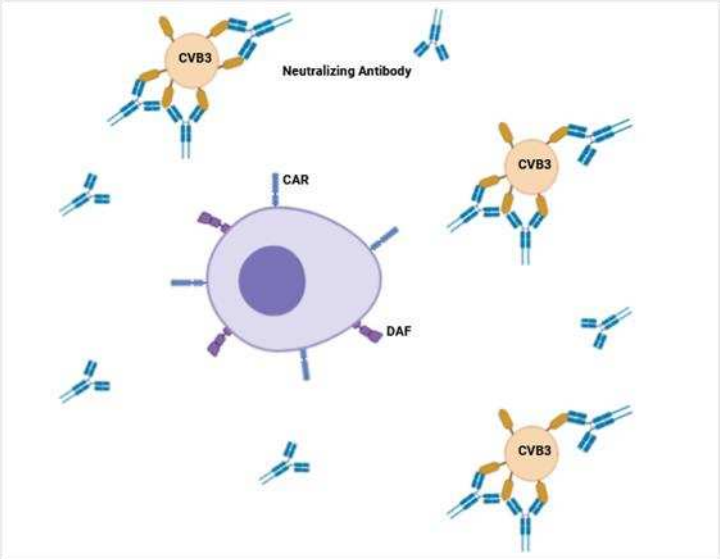

Figure 11: Mechanism of Neutralizing Antibody. Neutralizing antibodies target and bind to viral surface antigens. Once bound, neutralizing antibodies prevent free viruses from attaching to and entering host cells, effectively blocking the infection process. By inhibiting the virus's ability to interact with cell receptors, these antibodies stop the spread of the infection at its earliest stage. The figure was prepared with BioRender. CAR= coxsackievirus and adenovirus receptor, DAF= decay-accelerating factor.

Cells were followed for CPE daily. Detection of fluorescence in cells, a sign of successful GFP or sfCherry reassembly, meaning open ended cell contact formation was monitored on the 4th day using EVOS® FL Auto microscope. On

the 5th day the cells were fixed with 4% formaldehyde, added 100 µL PBS to keep the cells moist and stored at +4°C for further staining experiment.

2.8 Live imaging

A live imaging experiment was conducted using the EVOS® Onstage Incubator, which maintains optimal environmental conditions such as temperature, humidity, and CO_2 levels. 4-well chambered cover Glass with #1.5 glass-like polymer coverslip (Cellvis, C4-1.5P) was used. Cells were kept in the incubator overnight ($2x10^5$ cells/well) and infected with CVA9 and CVB3 diluted in infection media based on established MOI. The live experiment was conducted under optimal conditions in accordance with the manufacturer's guidelines. It was designed to run for 48h, with images captured at selected positions every 30 minutes, starting at the 24-hour mark. After which the cells were fixed with 4% formaldehyde.

3. Results

3.1 Optimization of methods and reagents

3.1.1 Selection of cell line, number of cells and virus amount

For virus stock preparation, all three cell lines were infected with CBV3, and it was found that GMK cells gave highest virus titers. Several experiments were done to determine the best number of cells and virus dilution for further experiments in 96-well plates. Cell amount used were $2x10^4$, $3x10^4$ and $4x10^4$/well. Each number of cells was infected with several serial virus dilutions, CVA9 with 10^{-2}, 10^{-3}, 10^{-4} and 10^{-5} as well as CVB3 with 10^{-4}, 10^{-5}, 10^{-6} and 10^{-7}. Which resulted in MOIs of 0.001-0.01 for both viruses. The first experiments were done using all three cell lines, but as both viruses grew best in GMK cells these were used for all further experiments. The virus infections were followed by formation of CPE in cells using a light microscope.

The number of cells used in further experiments were $3x10^4$ and $4x10^4$ cells/well in 96-well plates. The virus dilution used were CVA9 with 10^{-2}, 10^{-3} and CVB3 with 10^{-4}, 10^{-5}, which corresponded to MOIs of 0.01, 0.007 and 0.001, 0.0007 for both viruses.

3.1.2 Immunofluorescent staining

To find out the working concentration of antibodies and other small molecules, several experiments were done in black 96-well plate. Cells ($4x10^4$ cells/well) were infected with CVA9 and CVB3, both at MOIs 0.01 and 0.07. Antibodies, the concentrations tested, and optimal concentration are presented in Table 2. All four different enterovirus antibodies proved useful for our purposes. DAPI and PlasMem Bright Red were used at concentrations according to manufacturer's instructions.

Table 2: Used staining reagents, assessed and optimal concentrations.

Reagent name	Concentrations assessed	Optimal Conc.
Rabbit polyclonal anti-CVB3	1:250; 1:500; 1:1000	1:250
Rat anti-EV (3A6)	1:25; 1:50; 1:100	1:100
Mouse monoclonal anti-EV (5D8/1)	1:10; 1:25; 1:50	1:50
Mouse monoclonal anti-EV (9D5)	1:10; 1:25; 1:50; 1:100	1:100
Antibody for neutralization assay (Rabbit polyclonal anti-CVB3)	1:100; 1:200; 1:400; 1:800; 1:1600	1:400
Mouse monoclonal anti-dsRNA (mabJ2)	1:50; 1:100; 1:200	1:50
Phalloidin	1:20; 1:40	1:20

Table 3: Transfection reagents with the amounts assessed and the optimal amount for the best reagents.

Reagent name	Amounts of reagents assessed (µL)	Optimal amount (µL) to be used and comments
Lipofectamine-2000	2, 3, 4, and 5	2 Low transfection efficiency
Lipofectamine-3000	0.75 and 1.5	1.5 Best efficiency with consistent results
TransIT Lt1	1, 1.5, and 3	1 Best efficiency with consistent results
JetOPTIMUS	0.75 and 1	0.75 Not usable due to cytotoxicity
Transfectin	1, 1.5, and 2	Very low efficiency
Turbofect	1, 1.5, and 2	Very low efficiency
K2-transfection System	1.5, 2, and 2.5	2 Good efficiency with consistent results but complex protocol

3.1.3 Transfection

Several transfection reagents were assessed and optimized based on manufacturer's recommendation, reagents are listed in Table 3. The aim was to select the reagent which has maximum transfection efficiency and minimal cytotoxicity to GMK cells. Experiments were done on 24 well plates, using 0.5 µg EGFP-plasmid DNA mixed with transfection reagent in varying amounts and incubated for 48h. The development of green fluorescence in cells was monitored from 24h up to 48 hours using EVOS® FL Auto microscope.

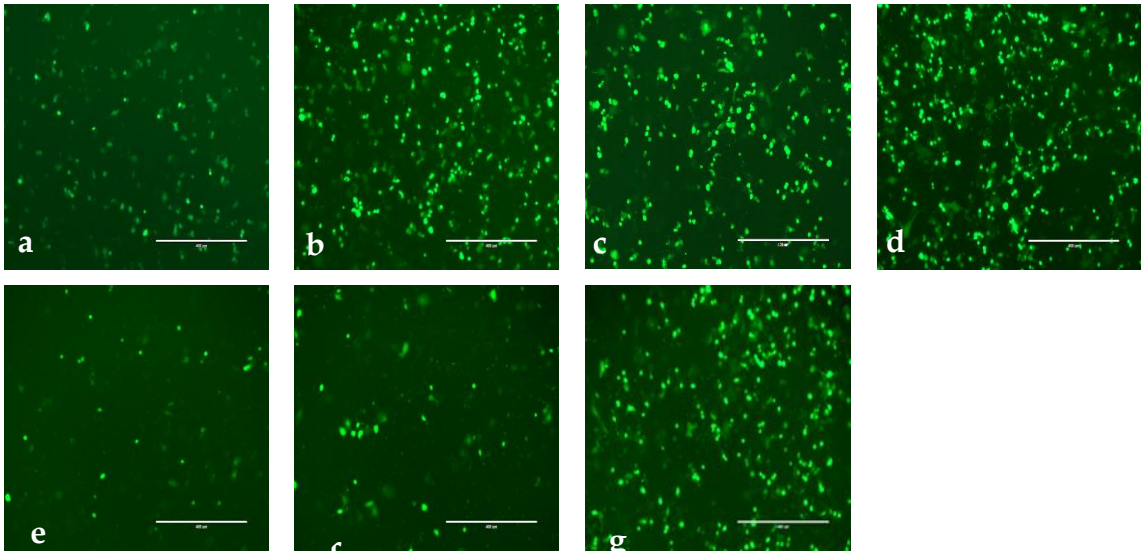

Figure 12: EGFP expression in GMK cells transfected with different transfection reagents with optimum amounts at 48h. (a) Lipofectamine-2000 (2 µL), (b) Lipofectamine-3000 (1.5 µL), (c) TransIT Lt1 (1 µL), (d) JetOPTIMUS (0.75 µL), (e) Transfectin (1.5 µL), (f) Turbofect (1 µL), (g) K2-transfection System (2 µL). Scale bar 200 µm.

The results in Figure 12 show that Lipofectamine-3000 (1.5 µL), TransIT-LT1 (1 µL), and the K2 Transfection System (2 µL) have the best transfection efficiency for GMK cells from the reagents tested. Although JetOPTIMUS (0.75 µL) also achieved efficient transfection, it exhibited a comparatively higher level of toxicity. Lipofectamine-3000 and TransIT-LT1 were selected for further transfection experiments with split GFP and split sfCherry.

3.1.4 Visualization of cellular connections utilizing split GFP technology

Split GFP and split sfCherry were employed to precisely visualize cell connections. The objective was to transfect cells with either the GFP1-10 or GFP11 containing plasmids, ensuring that fluorescence would only be observed if two cells, one containing GFP1-10 fragment and the other fragment GFP11, formed direct connections. Upon establishing such connections, the fragmented fluorescent proteins reassemble, emitting green fluorescence that is detectable with a microscope.

First both plasmids containing GFP1-10 and GFP11 fragments or sfCherry1-10 and sfCherry11 fragments were transfected into cells at the same time to ensure that there is fluorescence to be seen when the reassembly of split proteins takes place (Figure 13). The second step was to transfect each plasmid separately into cells in different wells (one well with GFP1-10, the second well with GFP11) and then co-culturing them to combine cells containing different fragments of the same protein. The third step was to add viral infection during this co-culture phase, to increase TNT formation. The fourth step was to add a neutralizing antibody after virus infection had proceeded for 4h. Thus, fluorescence would only be observed when transfected and infected cells establish direct open-ended cellular connections that also might allow viral transfer between them. To optimize the use of black walled plates and to save time, steps two to four were done on the same plate. Despite a few experiments and optimization, the expected results were not achieved. One likely explanation is the low transfection efficiency. Further optimization of transfection conditions and refinement for this experimental protocol are necessary to improve the success rate and ensure reliable detection of TNT formation.

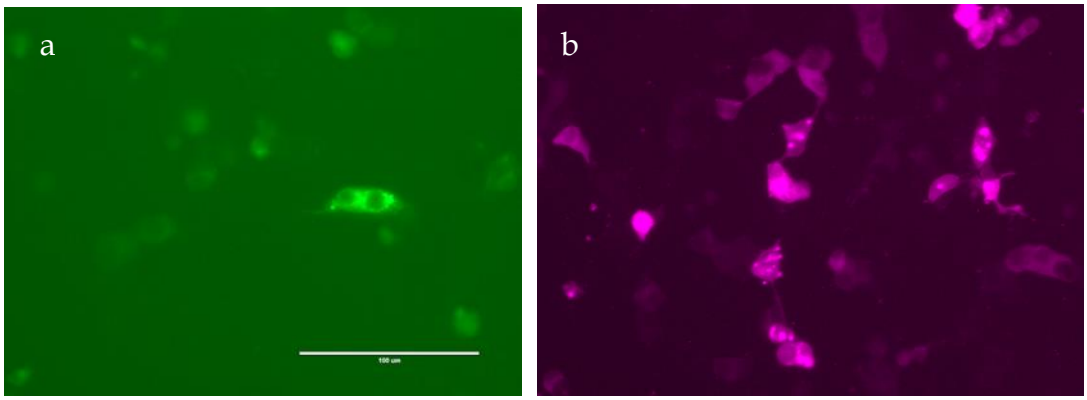

Figure 13: Cells transfected with split GFP or split sfCherry. Cells transfected using TransIT Lt1 reagent with plasmids carrying both (a) GFP1-10 and GFP11 or (b) sfCherry1-10 and sfCherry11-ß-actin. Images were taken after 48h, scale bar 100 µm.

3.2 Infection induced cell morphology changes

3.2.1 Formation of cellular protrusions

In the experiments, cellular protrusions connecting cells were observed under both stressed conditions and in the absence of infection. However, the number of these protrusions significantly increased when the cells were infected with CVA9 or CVB3. Although we could not definitively characterize these cellular protrusions, we will refer to them as tunneling nanotubes in the subsequent sections of this text.

Time-lapse imaging was used to analyse the time-dependent changes of cellular morphology (CPE) of CVA9 and CVB3 infected cells. Sequential images were captured at 30-minute intervals from 24 to 48h post-infection (pi). The virus infection induced CPE started to appear at 28.5h pi with cell rounding and shrinkage, which continued until 48h when all infected cells were dead. From 30h pi onward progressive morphological transformations and the emergence of filamentous protrusions were observed (Figure 14). These protrusions frequently established connections with neighbouring cells. However, the non-infected control cells also formed similar connections, to a lesser extent, and exhibited normal cell morphology while growing healthily.

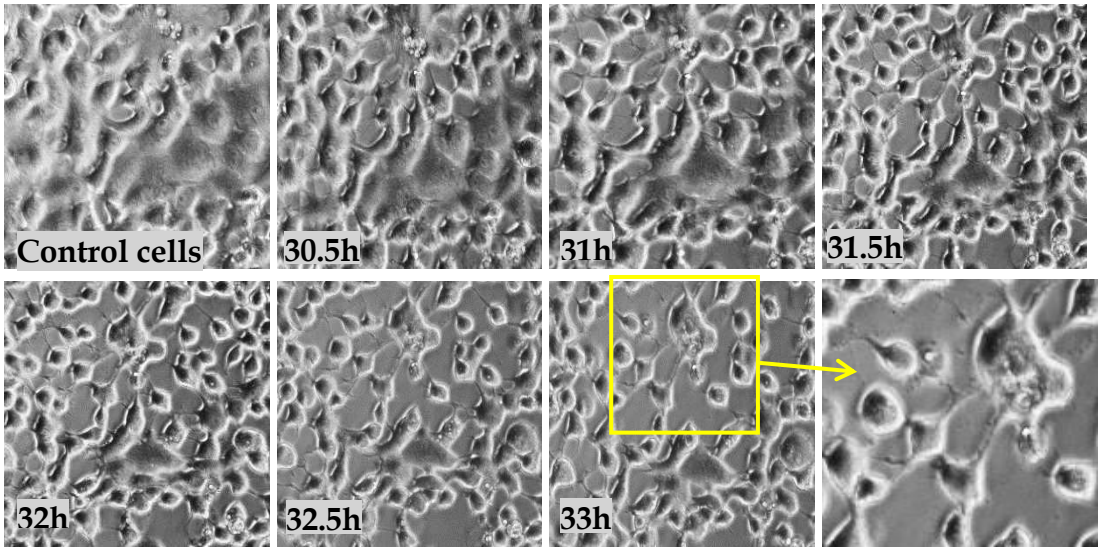

Figure 14: CVB3 infection-induced time-dependent changes in cell morphology. The images taken beginning 30h pi with half an hour interval show the gradual emergence of membranous protrusions.

The experiments detailed above demonstrate that infection with CVA9 and CVB3 significantly promotes the formation of cellular protrusions connecting adjacent cells. To further investigate these structures, staining was done to the infected cells for actin (showed in Figure 15), a key component present in TNTs.

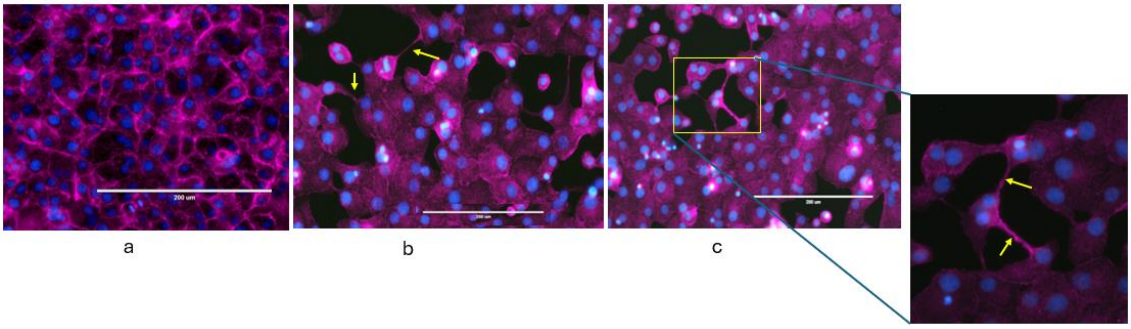

Figure 15: Infection induces cell protrusions. (a) Confluent control GMK cells. (b) & (c) 24h pi with CVA9 and CVB3, respectively. Phalloidin (red) was used to stain actin and DAPI (blue) for nucleus. Yellow arrows indicate protrusions (TNTs) connecting cells, containing actin. Scale bar, 200 µm.

3.2.2 Detection of viral protein, dsRNA, and cellular protrusions

Infected cells were fixed 24h after infection and stained with different antibodies detecting viral protein or dsRNA (Figure 16). Staining revealed

ongoing viral replication (presence of dsRNA), with clearly visible CPE. Imaging confirmed the presence of virus components within intercellular bridges between adjacent cells. However, at this stage, it remains uncertain whether these bridge-like structures are definitively open-ended TNTs or if viruses are spreading cell to cell through these cellular protrusions.

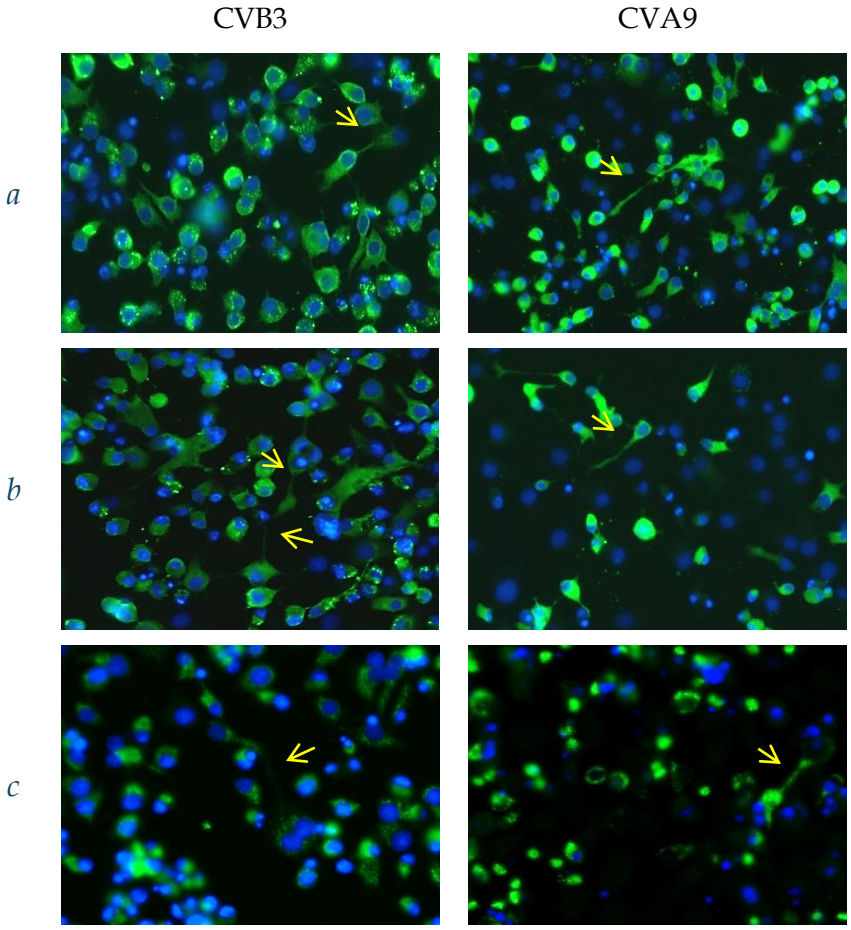

Figure 16: Viral replication in infected cells. Staining was done for viral protein using (a) rat anti-EV (3A6) (1:100), (b) mouse monoclonal anti-EV (5D8/1) (DAKO) (1:50) and for viral dsRNA using (c) mouse monoclonal anti-dsRNA (mabJ2) (1:50) 24h pi with CVB3 and CVA9. Nucleus was stained with DAPI in blue and viral components were stained in green. Yellow arrows point on the bridges made up of viral particles between the cells.

The high-magnification image in Figure 17 reveals cytoskeletal actin filaments (red) within the cellular protrusions (indicated by yellow arrows). Indicating that the protrusions could be TNTs. Additionally, viral protein (green) was

present in these structures, although to a lesser extent in this figure. Upon merging and analysing the fluorescence channels, it became more evident though not confirmed that the virus was utilizing these tunneling nanotubes as a pathway for cell-to-cell transmission.

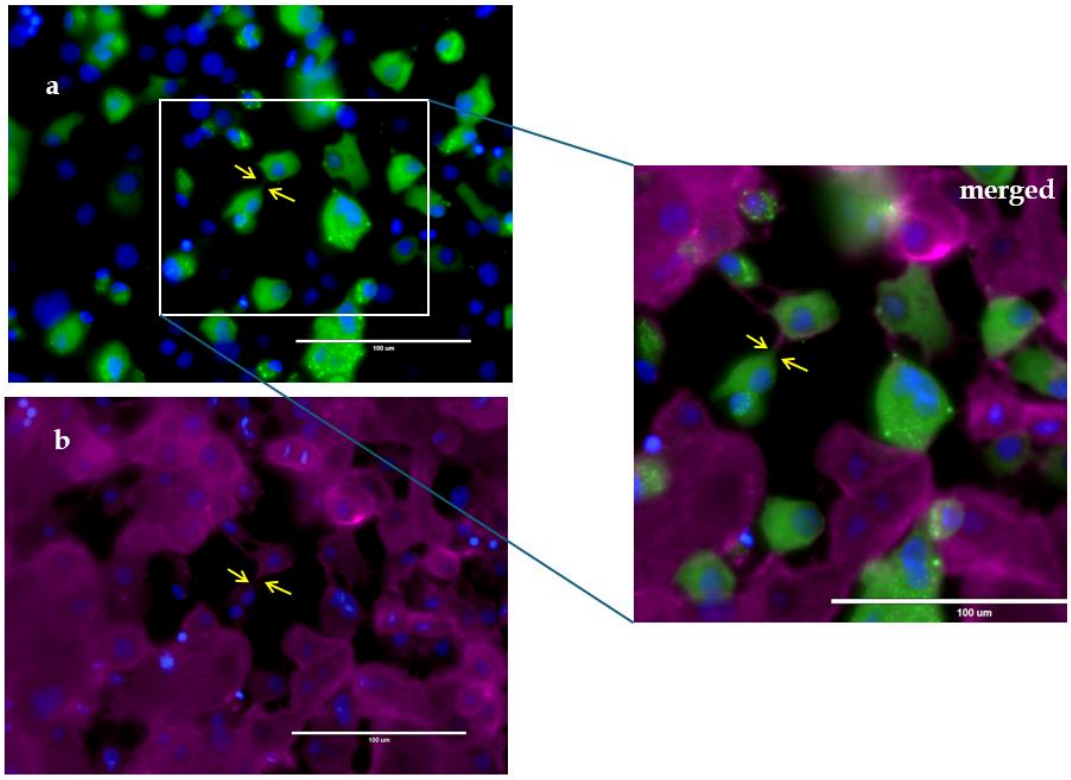

Figure 17: Cellular connections. Cells were infected with CBV3 and fixed at 24h pi. Staining was done for viral protein using rat anti-EV (3A6, green), Phalloidin was used to stain actin (red) and DAPI (blue) for nucleus staining. Scale bar, 100 µm.

3.3 Virus movement through TNTs

In the conducted experiments, high-magnification image analysis revealed distinct, continuous TNT-like structures connecting several cells, with an ongoing infection (Figure 18). Where it clearly looks like viral particles utilize these elongated tunnel formations to spread from one cell to another.

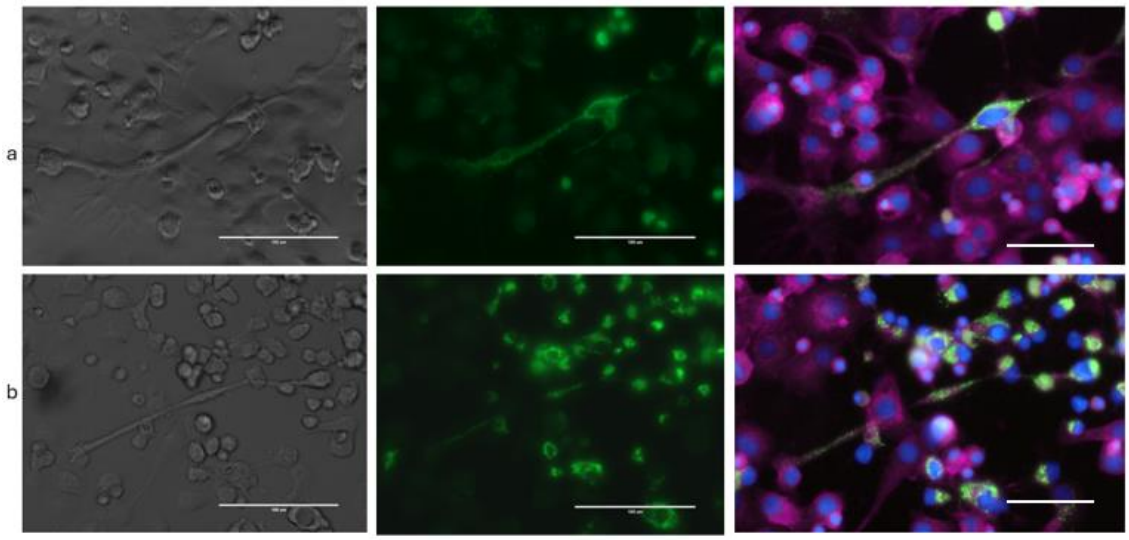

Figure 18: Viral spread via tunnels without cell rupture. The images presented in rows a and b depict two distinct regions of observation. The left column displays bright-field microscopy images, while the middle column shows green fluorescence images obtained using a mouse monoclonal anti-dsRNA antibody (mabJ2). The right column features merged images incorporating green fluorescence (anti-dsRNA), red fluorescence (cell membrane stained with PlasMem Bright Red), and blue fluorescence (nuclei stained with DAPI). Cells were infected with CBV3 and fixed at 24h pi. Scale bar, 100 μm.

The image clearly demonstrates that the plasma membrane envelops the entire tunnel-like structure composed of viral protein. This suggests that the virus does not rupture the infected cells to spread neighbouring, uninfected cells; instead, it appears to use these TNTs as a transmission pathway. When these specific wells containing TNT-like structures were stained with Phalloidin to assess actin distribution, it was unexpectedly observed that actin was minimally present in the infected cells. This observation needs further investigation. Additionally, to verify whether the tunnel-like structures are open-ended, split GFP technology was planned to be employed in separate experiments. However, this approach was unsuccessful, possibly due to limitations in transfection efficiency.

4. Discussion and Conclusion

In my study, I repeated some experiments done by Paloheimo *et al.,* 2011, which further continued to establish some new methodologies to find out possible route of enterovirus transmission from cell-to-cell. A big part of my work was to optimize reagents and split GFP technology to observe the virus induced morphological changes of cells. The study provides indications that TNTs serve as an alternative route for enterovirus transmission between cells. This novel mechanism contrasts sharply with the traditional understanding that enteroviruses primarily exit host cells through lysis and membrane disruption.

Findings from the study indicated, though not confirmed, that TNTs enable direct cell-to-cell viral transfer, potentially enhancing the efficiency of viral spread and persistence. TNTs are naturally occurring structures in cells, and studies have revealed that their formation may increase in response to some viral infection (Sowinski *et al.,* 2008; Gousset *et al.,* 2009; Kumar *et al.,* 2017). Similarly, my experiments demonstrated a significant increase in TNT formation among GMK cells upon infection with enterovirus. In the previous study, Paloheimo *et al.,* 2011 demonstrated that only CVB3, not CVA9, induces formation of TNTs in the morphology of GMK cells. However, microscopic analysis of infected cells in my study demonstrated that morphological alterations, including the emergence of actin-containing membranous protrusions was found with both CVA9 and CVB3 infections (Figure 16).

The study showed that virus-infected cells create thin extensions that connect them to other cells, and viral proteins were observed inside the extensions. However, we couldn't confirm whether these structures are open-ended thus enabling virus spread between cells. Since TNTs are delicate and complex, using a high-resolution microscope with advanced imaging capabilities is necessary to clearly see the detailed structures and connections they form between cells. This kind of imaging is important for understanding how TNTs help viruses spread. The split-GFP technology was used with the aim of direct

and extended real-time observation of cell fusions between cells infected with viruses. Achieving optimal results with this technology was hindered by low transfection efficiency of the cells, which presented a significant challenge throughout the experiment. In future experiments different cell lines can be used to face this problem. For example, with Huh-7 cells (a human liver cell line) a transfection efficiency of close to 100% can be achieved. Alternatively, a genetically engineered cell line having either GFP1-10 or GFP11 gene can be developed using lentiviral vectors or CRISPR-Cas technology, offering a stable and reliable alternative to traditional transfection experiments. Due to the time limit, these further experiments were not done.

In conclusion, this study aimed to design methodology to effectively demonstrate the mechanism of enterovirus transmission through tunneling nanotubes. A significant portion of the experimental time was dedicated to optimizing reagents and methods such as the neutralization experiment and split GFP technology, further experiments with more time are still required. The findings provide valuable insights into enteroviral pathogenesis and present new opportunities for exploring viral infection mechanisms. Although substantial progress has been made in understanding TNTs, further research is necessary to fully elucidate their roles across various pathological conditions. Such studies are essential for developing innovative therapeutic strategies targeting TNT-associated mechanisms for clinical applications.

References

Abounit, S. and Zurzolo, C., 2012. Wiring through tunneling nanotubes–from electrical signals to organelle transfer. Journal of cell science, 125(5), pp.1089-1098.

Alzahrani, T., Eftimie, R. and Trucu, D., 2020. Multiscale moving boundary modelling of cancer interactions with a fusogenic oncolytic virus: the impact of syncytia dynamics. Mathematical Biosciences, 323, p.108296.

Ariazi, J., Benowitz, A., De Biasi, V., Den Boer, M.L., Cherqui, S., Cui, H., Douillet, N., Eugenin, E.A., Favre, D., Goodman, S. and Gousset, K., 2017. Tunneling nanotubes and gap junctions–their role in long-range intercellular communication during development, health, and disease conditions. Frontiers in molecular neuroscience, 10, p.333.

Aubry, C., Gautret, P., Nougairede, A., Dussouil, A.S., Botelho-Nevers, E., Zandotti, C., De Lamballerie, X., Brouqui, P. and Parola, P., 2012. 2012 outbreak of acute haemorrhagic conjunctivitis in Indian Ocean Islands: identification of Coxsackievirus A24 in a returned traveller. Eurosurveillance, 17(22), p.20185.

Baggen, J., Thibaut, H.J., Staring, J., Jae, L.T., Liu, Y., Guo, H., Slager, J.J., de Bruin, J.W., van Vliet, A.L., Blomen, V.A. and Overduin, P., 2016. Enterovirus D68 receptor requirements unveiled by haploid genetics. Proceedings of the national academy of sciences, 113(5), pp.1399-1404.

Baggen, J., Thibaut, H.J., Strating, J.R. and van Kuppeveld, F.J., 2018. The life cycle of non-polio enteroviruses and how to target it. Nature Reviews Microbiology, 16(6), pp.368-381.

Barnadas, C., Midgley, S.E., Skov, M.N., Jensen, L., Poulsen, M.W. and Fischer, T.K., 2017. An enhanced Enterovirus surveillance system allows identification and characterization of rare and emerging respiratory enteroviruses in Denmark, 2015–16. Journal of Clinical Virology, 93, pp.40-44.

Bergelson, J.M., Cunningham, J.A., Droguett, G., Kurt-Jones, E.A., Krithivas, A., Hong, J.S., Horwitz, M.S., Crowell, R.L. and Finberg, R.W., 1997. Isolation of a common receptor for Coxsackie B viruses and adenoviruses 2 and 5. Science, 275(5304), pp.1320-1323.

Bergelson, J.M., Mohanty, J.G., Crowell, R.L., St John, N.F., Lublin, D.M. and Finberg, R.W., 1995. Coxsackievirus B3 adapted to growth in RD cells binds to decay-accelerating factor (CD55). Journal of virology, 69(3), pp.1903-1906.

Bird, S.W., Maynard, N.D., Covert, M.W. and Kirkegaard, K., 2014. Nonlytic viral spread enhanced by autophagy components. Proceedings of the National Academy of Sciences, 111(36), pp.13081-13086.

Bubba, L., Broberg, E.K., Jasir, A., Simmonds, P., Harvala, H., Redlberger-Fritz, M., Nikolaeva-Glomb, L., Havlíčková, M., Rainetova, P., Fischer, T.K. and Midgley, S.E., 2020. Circulation of non-polio enteroviruses in 24 EU and EEA countries between 2015 and 2017: a retrospective surveillance study. The Lancet Infectious Diseases, 20(3), pp.350-361.

Buchrieser, J., Dufloo, J., Hubert, M., Monel, B., Planas, D., Rajah, M.M., Planchais, C., Porrot, F., Guivel-Benhassine, F., Van der Werf, S. and Casartelli, N., 2020. Syncytia formation by SARS-CoV-2-infected cells. The EMBO journal, 39(23), p.e106267.

Chen, N., Zhou, M., Dong, X., Qu, J., Gong, F., Han, Y., Qiu, Y., Wang, J., Liu, Y., Wei, Y. and Yu, T., 2020. Epidemiological and clinical characteristics of 99 cases of 2019 novel coronavirus pneumonia in Wuhan, China: a descriptive study. The lancet, 395(10223), pp.507-513.

Chen, Y.H., Du, W., Hagemeijer, M.C., Takvorian, P.M., Pau, C., Cali, A., Brantner, C.A., Stempinski, E.S., Connelly, P.S., Ma, H.C. and Jiang, P., 2015. Phosphatidylserine vesicles enable efficient en bloc transmission of enteroviruses. Cell, 160(4), pp.619-630.

Chia, M.Y., Chiang, P.S., Chung, W.Y., Luo, S.T. and Lee, M.S., 2014. Epidemiology of enterovirus 71 infections in Taiwan. Pediatrics & Neonatology, 55(4), pp.243-249.

Chong, P., Liu, C.C., Chow, Y.H., Chou, A.H. and Klein, M., 2015. Review of enterovirus 71 vaccines. Clinical Infectious Diseases, 60(5), pp.797-803.

Cieri, D., Vicario, M., Giacomello, M., Vallese, F., Filadi, R., Wagner, T., Pozzan, T., Pizzo, P., Scorrano, L., Brini, M. and Calì, T., 2018. SPLICS: a split green fluorescent protein-based contact site sensor for narrow and wide heterotypic organelle juxtaposition. Cell Death & Differentiation, 25(6), pp.1131-1145.

Cifuentes-Muñoz, N., Dutch, R.E. and Cattaneo, R., 2018. Direct cell-to-cell transmission of respiratory viruses: The fast lanes. PLoS pathogens, 14(6), p.e1007015.

Cifuentes-Munoz, N., El Najjar, F. and Dutch, R.E., 2020. Viral cell-to-cell spread: Conventional and non-conventional ways. Advances in virus research, 108, pp.85-125.

Cole, N.L. and Grose, C., 2003. Membrane fusion mediated by herpesvirus glycoproteins: the paradigm of varicella-zoster virus. Reviews in medical virology, 13(4), pp.207-222.

Desir, S., O'Hare, P., Vogel, R.I., Sperduto, W., Sarkari, A., Dickson, E.L., Wong, P., Nelson, A.C., Fong, Y., Steer, C.J. and Subramanian, S., 2018. Chemotherapy-induced tunneling nanotubes mediate intercellular drug efflux in pancreatic cancer. Scientific reports, 8(1), p.9484.

Dewhirst, M.W. and Secomb, T.W., 2017. Transport of drugs from blood vessels to tumour tissue. Nature Reviews Cancer, 17(12), pp.738-750.

Dupont, M. and Sattentau, Q.J., 2020. Macrophage cell-cell interactions promoting HIV-1 infection. Viruses, 12(5), p.492.

Eugenin, E.A., Gaskill, P.J. and Berman, J.W., 2009. Tunneling nanotubes (TNT) are induced by HIV-infection of macrophages: a potential mechanism for intercellular HIV trafficking. Cellular immunology, 254(2), pp.142-148.

Feng, Z., Hensley, L., McKnight, K.L., Hu, F., Madden, V., Ping, L., Jeong, S.H., Walker, C., Lanford, R.E. and Lemon, S.M., 2013. A pathogenic picornavirus acquires an envelope by hijacking cellular membranes. Nature, 496(7445), pp.367-371.

Gerdes, H.H., Rustom, A. and Wang, X., 2013. Tunneling nanotubes, an emerging intercellular communication route in development. Mechanisms of development, 130(6-8), pp.381-387.

Giorda, K.M. and Hebert, D.N., 2013. Viroporins customize host cells for efficient viral propagation. DNA and cell biology, 32(10), pp.557-564.

Gousset, K., Schiff, E., Langevin, C., Marijanovic, Z., Caputo, A., Browman, D.T., Chenouard, N., De Chaumont, F., Martino, A., Enninga, J. and Olivo-Marin, J.C., 2009. Prions hijack tunnelling nanotubes for intercellular spread. Nature cell biology, 11(3), pp.328-336.

Greve, J.M., Davis, G., Meyer, A.M., Forte, C.P., Yost, S.C., Marlor, C.W., Kamarck, M.E. and McClelland, A., 1989. The major human rhinovirus receptor is ICAM-1. Cell, 56(5), pp.839-847.

Hanna, S.J., McCoy-Simandle, K., Leung, E., Genna, A., Condeelis, J. and Cox, D., 2019. Tunneling nanotubes, a novel mode of tumor cell–macrophage communication in tumor cell invasion. Journal of cell science, 132(3), p.jcs223321.

Hashimoto, M., Bhuyan, F., Hiyoshi, M., Noyori, O., Nasser, H., Miyazaki, M., Saito, T., Kondoh, Y., Osada, H., Kimura, S. and Hase, K., 2016. Potential role of the formation of tunneling nanotubes in HIV-1 spread in macrophages. The Journal of Immunology, 196(4), pp.1832-1841.

Ilyichev, A.A., Orlova, L.A., Sharabrin, S.V. and Karpenko, L.I., 2020. mRNA technology as one of the promising platforms for the SARS-CoV-2 vaccine development. Vavilov Journal of Genetics and Breeding, 24(7), p.802.

Johnson, F.H., Shimomura, O., Saiga, Y., Gershman, L.C., Reynolds, G.T. and Waters, J.R., 1962. Quantum efficiency of Cypridina luminescence, with a note on that of Aequorea. Journal of Cellular and Comparative Physiology, 60(1), pp.85-103.

Kamiyama, D., Sekine, S., Barsi-Rhyne, B., Hu, J., Chen, B., Gilbert, L.A., Ishikawa, H., Leonetti, M.D., Marshall, W.F., Weissman, J.S. and Huang, B., 2016. Versatile protein tagging in cells with split fluorescent protein. Nature communications, 7(1), p.11046.

Kent, K.P., Childs, W. and Boxer, S.G., 2008. Deconstructing green fluorescent protein. Journal of the American Chemical Society, 130(30), pp.9664-9665.

Khan, F., 2015. Enterovirus D68: acute respiratory illness and the 2014 outbreak. Emergency Medicine Clinics, 33(2), pp.e19-e32.

Khetsuriani, N., LaMonte-Fowlkes, A., Oberst, S., Pallansch, M.A. and Centers for Disease Control and Prevention, 2006. Enterovirus surveillance—United States, 1970–2005. MMWR Surveill Summ, 55(8), pp.1-20.

Koyanagi, M., Brandes, R.P., Haendeler, J., Zeiher, A.M. and Dimmeler, S., 2005. Cell-to-cell connection of endothelial progenitor cells with cardiac myocytes by nanotubes: a novel mechanism for cell fate changes?. Circulation research, 96(10), pp.1039-1041.

Kumar, A., Kim, J.H., Ranjan, P., Metcalfe, M.G., Cao, W., Mishina, M., Gangappa, S., Guo, Z., Boyden, E.S., Zaki, S. and York, I., 2017. Influenza virus exploits tunneling nanotubes for cell-to-cell spread. Scientific reports, 7(1), p.40360.

Laitinen, O.H., Svedin, E., Kapell, S., Nurminen, A., Hytönen, V.P. and Flodström-Tullberg, M., 2016. Enteroviral proteases: structure, host interactions and pathogenicity. Reviews in medical virology, 26(4), pp.251-267.

Leroy, H., Han, M., Woottum, M., Bracq, L., Bouchet, J., Xie, M. and Benichou, S., 2020. Virus-mediated cell-cell fusion. International Journal of Molecular Sciences, 21(24), p.9644.

Lorizate, M. and Kräusslich, H.G., 2011. Role of lipids in virus replication. Cold Spring Harbor perspectives in biology, 3(10), p.a004820.

Mendelsohn, C.L., Wimmer, E. and Racaniello, V.R., 1989. Cellular receptor for poliovirus: molecular cloning, nucleotide sequence, and expression of a new member of the immunoglobulin superfamily. Cell, 56(5), pp.855-865.

Morise, H., Shimomura, O., Johnson, F.H. and Winant, J., 1974. Intermolecular energy transfer in the bioluminescent system of Aequorea. Biochemistry, 13(12), pp.2656-2662.

Nguyen, H.B., Hung, L.W., Yeates, T.O., Terwilliger, T.C. and Waldo, G.S., 2013. Split green fluorescent protein as a modular binding partner for protein crystallization. Acta Crystallographica Section D: Biological Crystallography, 69(12), pp.2513-2523.

Nieva, J.L., Madan, V. and Carrasco, L., 2012. Viroporins: structure and biological functions. Nature Reviews Microbiology, 10(8), pp.563-574.

Nkosi, N., Preiser, W., Van Zyl, G., Claassen, M., Cronje, N., Maritz, J., Newman, H., McCarthy, K., Ntshoe, G., Essel, V. and Korsman, S., 2021. Molecular characterisation and epidemiology of enterovirus-associated aseptic meningitis in the Western and Eastern Cape Provinces, South Africa 2018–2019. Journal of Clinical Virology, 139, p.104845.

Nomoto, A., 2007. Molecular aspects of poliovirus pathogenesis. Proceedings of the Japan Academy, Series B, 83(8), pp.266-275.

Oberste, M.S., Maher, K. and Pallansch, M.A., 2002. Molecular phylogeny and proposed classification of the simian picornaviruses. Journal of virology, 76(3), pp.1244-1251.

Omsland, M., Bruserud, Ø., Gjertsen, B.T. and Andresen, V., 2017. Tunneling nanotube (TNT) formation is downregulated by cytarabine and NF-κB inhibition in acute myeloid leukemia (AML). Oncotarget, 8(5), p.7946.

Ormö, M., Cubitt, A.B., Kallio, K., Gross, L.A., Tsien, R.Y. and Remington, S.J., 1996. Crystal structure of the Aequorea victoria green fluorescent protein. Science, 273(5280), pp.1392-1395.

Palacios, G. and Oberste, M.S., 2005. Enteroviruses as agents of emerging infectious diseases. Journal of neurovirology, 11(5), pp.424-433.

Pallansch M.A., Oberste M.S., Whitton J.L., 2013. In: Field's Virology. 6th ed. Knipe D., Howley P., Cohen J., Lamb R., Martin M., Racaniello V., Roizman B., editors. Wolters Kluwer/Lippincott Williams & Wilkins Health; Philadelpha, PA, USA.

Pallansch, M.A.R.R., 2006. Enteroviruses: polioviruses, coxsackieviruses, echoviruses, and newer enteroviruses. Fields virology, 1, pp.840-867.

Paloheimo, O., Ihalainen, T.O., Tauriainen, S., Välilehto, O., Kirjavainen, S., Niskanen, E.A., Laakkonen, J.P., Hyöty, H. and Vihinen-Ranta, M., 2011. Coxsackievirus B3-induced cellular protrusions: structural characteristics and functional competence. Journal of virology, 85(13), pp.6714-6724.

Panasiuk, M., Rychłowski, M., Derewońko, N. and Bieńkowska-Szewczyk, K., 2018. Tunneling nanotubes as a novel route of cell-to-cell spread of herpesviruses. Journal of virology, 92(10), pp.10-1128.

Pepe, A., Pietropaoli, S., Vos, M., Barba-Spaeth, G. and Zurzolo, C., 2022. Tunneling nanotubes provide a route for SARS-CoV-2 spreading. Science Advances, 8(29), p.eabo0171.

Perozzo, M.A., Ward, K.B., Thompson, R.B. and Ward, W.W., 1988. X-ray diffraction and time-resolved fluorescence analyses of Aequorea green fluorescent protein crystals. Journal of Biological Chemistry, 263(16), pp.7713-7716.

Pons-Salort, M. and Grassly, N.C., 2018. Serotype-specific immunity explains the incidence of diseases caused by human enteroviruses. Science, 361(6404), pp.800-803.

Reed, L.J. and Muench, H., 1938. A simple method of estimating fifty per cent endpoints.

Ren, R.U.I.B.A.O. and Racaniello, V.R., 1992. Human poliovirus receptor gene expression and poliovirus tissue tropism in transgenic mice. Journal of virology, 66(1), pp.296-304.

Roberts, K.L., Manicassamy, B. and Lamb, R.A., 2015. Influenza A virus uses intercellular connections to spread to neighboring cells. Journal of virology, 89(3), pp.1537-1549.

Rustom, A., Saffrich, R., Markovic, I., Walther, P. and Gerdes, H.H., 2004. Nanotubular highways for intercellular organelle transport. Science, 303(5660), pp.1007-1010.

Santiana, M., Ghosh, S., Ho, B.A., Rajasekaran, V., Du, W.L., Mutsafi, Y., De Jésus-Diaz, D.A., Sosnovtsev, S.V., Levenson, E.A., Parra, G.I. and

Takvorian, P.M., 2018. Vesicle-cloaked virus clusters are optimal units for inter-organismal viral transmission. Cell host & microbe, 24(2), pp.208-220.

Sartori-Rupp, A., Cordero Cervantes, D., Pepe, A., Gousset, K., Delage, E., Corroyer-Dulmont, S., Schmitt, C., Krijnse-Locker, J. and Zurzolo, C., 2019. Correlative cryo-electron microscopy reveals the structure of TNTs in neuronal cells. Nature communications, 10(1), p.342.

Scully, E.P., Haverfield, J., Ursin, R.L., Tannenbaum, C. and Klein, S.L., 2020. Considering how biological sex impacts immune responses and COVID-19 outcomes. Nature Reviews Immunology, 20(7), pp.442-447.

Shaner, N.C., Campbell, R.E., Steinbach, P.A., Giepmans, B.N., Palmer, A.E. and Tsien, R.Y., 2004. Improved monomeric red, orange and yellow fluorescent proteins derived from Discosoma sp. red fluorescent protein. Nature biotechnology, 22(12), pp.1567-1572.

Shimomura, O., Johnson, F.H. and Saiga, Y., 1962. Extraction, purification and properties of aequorin, a bioluminescent protein from the luminous hydromedusan, Aequorea. Journal of cellular and comparative physiology, 59(3), pp.223-239.

Shu, X., Shaner, N.C., Yarbrough, C.A., Tsien, R.Y. and Remington, S.J., 2006. Novel chromophores and buried charges control color in mFruits. Biochemistry, 45(32), pp.9639-9647.

Simmonds, P., Gorbalenya, A.E., Harvala, H., Hovi, T., Knowles, N.J., Lindberg, A.M., Oberste, M.S., Palmenberg, A.C., Reuter, G., Skern, T. and Tapparel, C., 2020. Recommendations for the nomenclature of enteroviruses and rhinoviruses. Archives of virology, 165, pp.793-797.

Souriant, S., Balboa, L., Dupont, M., Pingris, K., Kviatcovsky, D., Cougoule, C., Lastrucci, C., Bah, A., Gasser, R., Poincloux, R. and Raynaud-Messina, B., 2019. Tuberculosis exacerbates HIV-1 infection through IL-10/STAT3-dependent tunneling nanotube formation in macrophages. Cell reports, 26(13), pp.3586-3599.

Sowinski, S., Jolly, C., Berninghausen, O., Purbhoo, M.A., Chauveau, A., Köhler, K., Oddos, S., Eissmann, P., Brodsky, F.M., Hopkins, C. and Önfelt, B., 2008.

Membrane nanotubes physically connect T cells over long distances presenting a novel route for HIV-1 transmission. Nature cell biology, 10(2), pp.211-219.

Staring, J., van den Hengel, L.G., Raaben, M., Blomen, V.A., Carette, J.E. and Brummelkamp, T.R., 2018. KREMEN1 is a host entry receptor for a major group of enteroviruses. Cell Host & Microbe, 23(5), pp.636-643.

Tiwari, V., Koganti, R., Russell, G., Sharma, A. and Shukla, D., 2021. Role of tunneling nanotubes in viral infection, neurodegenerative disease, and cancer. Frontiers in Immunology, 12, p.680891.

Torres, S.D., Jia, D.T., Schorr, E.M., Park, B.L., Boubour, A., Boehme, A., Ankam, J.V., Gofshteyn, J.S., Tyshkov, C., Green, D.A. and Vargas, W., 2020. Central nervous system (CNS) enterovirus infections: A single center retrospective study on clinical features, diagnostic studies, and outcome. Journal of neurovirology, 26, pp.14-22.

Tsien, R.Y., 1998. The green fluorescent protein. Annual review of biochemistry, 67(1), pp.509-544.

Vignais, M.L., Caicedo, A., Brondello, J.M. and Jorgensen, C., 2017. Cell connections by tunneling nanotubes: effects of mitochondrial trafficking on target cell metabolism, homeostasis, and response to therapy. Stem cells international, 2017(1), p.6917941.

Wang, X. and Gerdes, H.H., 2015. Transfer of mitochondria via tunneling nanotubes rescues apoptotic PC12 cells. Cell Death & Differentiation, 22(7), pp.1181-1191.

Wang, X.T., Sun, H., Chen, N.H. and Yuan, Y.H., 2021. Tunneling nanotubes: A novel pharmacological target for neurodegenerative diseases?. Pharmacological Research, 170, p.105541.

Weissenhorn, W., Poudevigne, E., Effantin, G. and Bassereau, P., 2013. How to get out: ssRNA enveloped viruses and membrane fission. Current opinion in virology, 3(2), pp.159-167.

Yamashita, Y.M., Inaba, M. and Buszczak, M., 2018. Specialized intercellular communications via cytonemes and nanotubes. Annual review of cell and developmental biology, 34(1), pp.59-84.

Yea, C., Bitnun, A., Branson, H.M., Ciftci-Kavaklioglu, B., Rafay, M.F., Fortin, O., Moresoli, P., Sébire, G., Srour, M., Decaluwe, H. and Marois, L., 2020. Association of outcomes in acute flaccid myelitis with identification of enterovirus at presentation: a Canadian, nationwide, longitudinal study. The Lancet Child & Adolescent Health, 4(11), pp.828-836.

Zhu, F., Xu, W., Xia, J., Liang, Z., Liu, Y., Zhang, X., Tan, X., Wang, L., Mao, Q., Wu, J. and Hu, Y., 2014. Efficacy, safety, and immunogenicity of an enterovirus 71 vaccine in China. New England Journal of Medicine, 370(9), pp.818-828.

Zurzolo, C., 2021. Tunneling nanotubes: Reshaping connectivity. Current opinion in cell biology, 71, pp.139-147.

Acknowledgement

I am grateful to my supervisor, Dr. Sisko Tauriainen (Docent) for providing me the opportunity to work in the project, her continuous guidance, insightful advice, and patience throughout my research journey and thesis writing. I express my indebtedness for her exceptional support, which extended beyond academic mentorship to personal encouragement and assistance in my life.

I am also sincerely thankful to my co-supervisor, Dr. Petri Susi (Docent), for entrusting me with this project and providing unwavering support in every aspect of my work. His expertise and encouragement have played a crucial role in the successful completion of this research.

I extend my heartfelt gratitude to Professor Paula Mulo, for providing invaluable guidance regarding all course work and her support in addressing challenges I faced throughout my study period.

Cordial thanks to Professor Ilkka Julkunen's group and all the lab members of Medisiina D 7th floor for the kind co-operation during the period of thesis work.

Finally, I wish to acknowledge my parents and my younger brother for their unconditional love, supporting and pushing me towards my dream. Their belief in my abilities has been a pillar of strength throughout my studies.

Sayma Farabi
December 2024